METABOLISM *IN VITRO* OF THE MICROTUBULE PERTURBAGENS: CERATAMINES A AND B

by

Sara Elizabeth Smith

Bachelor of Science, Chemistry, Pennsylvania State University, 2008

Master of Professional Studies, Forensic Science, Pennsylvania State University, 2010

Submitted to the Graduate Faculty of the

Kenneth P. Dietrich School of Arts and Sciences in partial fulfillment

of the requirements for the degree of

Doctor of Philosophy in Chemistry

University of Pittsburgh

2014

UNIVERSITY OF PITTSBURGH

DIETRICH SCHOOL OF ARTS AND SCIENCES

This dissertation was presented

by

Sara Elizabeth Smith

It was defended on

July 30, 2014

and approved by

Xinyu Liu, Assistant Professor, Department of Chemistry

Samuel M. Poloyac, Associate Professor, Department of Pharmaceutical Sciences

Renã A. S. Robinson, Assistant Professor, Department of Chemistry

Dissertation Advisor: Stephen G. Weber, Professor, Department of Chemistry

METABOLISM *IN VITRO* OF THE MICROTUBULE PERTURBAGENS: CERATAMINES A AND B

Sara E. Smith, PhD

University of Pittsburgh, 2014

Ceratamines A and B are heterocyclic alkaloids isolated from a *Pseudoceratina* sp. marine sponge. These natural products behave as antimitotic agents by targeting microtubules, specifically through a stabilization mechanism. Their identification led to the discovery of a novel class of structurally simple microtubule stabilizers, with implications in the treatment of cancer and perhaps tauopathies, including Alzheimer's disease. To date, no pre-clinical studies of the ceratamines have been reported. Therefore, I determined the phase I metabolism of each compound *in vitro*. Ceratamine A is rapidly metabolized into nine phase I metabolites by rat liver microsomes, while ceratamine B only yielded five metabolites. The majority of these metabolites were formed as a result of *N*- and *O*-dealkylations. While the metabolites formed from both compounds were similar when incubated with human liver microsomes, the major metabolites were not the same as those from rat liver microsomes. The aminoimidazole is the most metabolically labile site in rat liver microsomes, however the dibrominated aromatic moiety is the preferred site for metabolism in human liver microsomes. A metabolic stability assay revealed that both compounds have a high estimated clearance in rat liver microsomes, but they appear to be more stable in human liver microsomes. Ceratamine B was estimated to have a moderate clearance, while ceratamine A was found to have a low clearance. Finally, isozyme mapping and small molecule inhibition studies revealed that the specific P450 isoforms

responsible for the formation of two major metabolites of ceratamine B in human liver microsomes is CYP3A4/5.

TABLE OF CONTENTS

TABLE OF CONTENTS VI

LIST OF TABLES……X

LIST OF FIGURES XII

ABBREVIATIONS XVI

1.0 INTRODUCTION 1

1.1 MARINE NATURAL PRODUCTS IN DRUG DISCOVERY 1

1.2 ANTIMITOTIC NATURAL PRODUCTS 2

1.3 CLINICAL SIGNIFICANCE OF MICROTUBULE PERTURBAGENS... 10

1.4 CERATAMINES A AND B 12

1.5 PROJECT GOALS 16

1.6 METABOLISM 17

1.6.1 Introduction to xenobiotic metabolism 17

1.6.2 *In vitro* metabolism studies 19

2.0 EXPERIMENTAL 24

2.1 MATERIALS 24

2.2 METHODS 25

2.2.1 Microsomal incubations 25

2.2.2 Large scale microsomal incubations 25

2.2.3 Species comparison 26

2.2.4 Metabolic stability assay 26

2.2.5 Incubations of ceratamine B with 1-aminobenzotriazole 27

2.2.6 Incubations of ceratamine B with recombinant P450 isoforms 27

2.2.7 Incubations of ceratamine B with small molecule inhibitors 28

2.3 ANALYSIS 28

2.3.1 HPLC-UV analysis 28

2.3.2 LC-MS/MS analysis 29

2.3.3 UV/Vis analysis 35

2.3.4 ^{1}H NMR analysis 35

3.0 STRUCTURE ELUCIDATION OF PHASE I METABOLITES OF THE MICROTUBULE PERTURBAGENS: CERATAMINES A AND B 36

3.1 PHASE I METABOLISM OF CERATAMINES A AND B IN RAT LIVER MICROSOMES 36

3.2 PRELIMINARY STRUCTURE ELUCIDATION OF PHASE I METABOLITES OF CERATAMINES A AND B 37

3.2.1 MS spectra of ceratamines A and B 37

3.2.2 Metabolites of ceratamine B 39

3.2.3 Metabolites of ceratamine A 43

3.2.4 Multiple reaction monitoring of metabolites of the ceratamines 50

3.3 CONFIRMATORY STRUCTURE ELUCIDATION OF PHASE I METABOLITES OF CERATAMINES A AND B 53

3.3.1 Co-injection experiment 53

3.3.2 Accurate mass determinations 54

3.3.3 Isolation of major metabolites of ceratamine B 55

3.3.4 UV/Vis spectroscopy 57

3.3.5 ^{1}H NMR spectroscopy 59

4.0 SPECIES COMPARISON OF METABOLIC PROFILE AND STABILITY OF THE MICROTUBULE PERTURBAGENS: CERATAMINES A AND B 62

4.1 SEMI-QUANTITATIVE EVALUATION OF THE METABOLISM OF THE CERATAMINES IN RAT LIVER MICROSOMES 62

4.2 SEMI-QUANTITATIVE EVALUATION OF THE METABOLISM OF THE CERATAMINES IN HUMAN LIVER MICROSOMES 64

4.3 SPECIES DIFFERENCES IN THE METABOLISM OF THE CERATAMINES 72

4.4 METABOLIC STABILITY OF THE CERATAMINES 74

4.4.1 Metabolic stability of the ceratamines in rat liver microsomes 75

4.4.2 Metabolic stability of the ceratamines in human liver microsomes 78

5.0 IDENTIFICATION OF CYTOCHROMES P450 ISOFORMS INVOLVED IN HUMAN PHASE I METABOLISM OF CERATAMINE B 81

5.1 OPTIMIZATION OF CONDITIONS FOR SMALL MOLECULE INHIBITOR STUDIES 82

5.2 EFFECT OF 1-AMINOBENZOTRIAZOLE ON THE HUMAN PHASE I METABOLISM OF CERATAMINE B 85

5.3 IDENTIFICATION OF P450 ISOFORMS INVOLVED IN THE FORMATION OF M3 AND M4 88

5.3.1 Isozyme mapping 88

5.3.2 Small molecule inhibition studies 89

6.0 CONCLUSION 91

7.0 FUTURE DIRECTIONS 93

APPENDIX A 95

REFERENCES 99

LIST OF TABLES

Table 1.1 Cytochrome P450 isoforms involved in xenobiotic metabolism..... 18

Table 2.1 MS-MS source parameters used for the analysis of the ceratamines and the metabolic stability control compounds……...30

Table 2.2 Additional MS-MS source parameters used for the analysis of the ceratamines and the metabolic stability control compounds……...……...31

Table 2.3 MS-MS compound parameters used for the analysis of the ceratamines and the metabolic stability control compounds ……..……..….32

Table 2.4 Additional MS-MS compound parameters used for the analysis of the ceratamines and the metabolic stability control compounds ……..……..……..….33

Table 3.1 Chromatographic and mass spectrometric information of metabolites of ceratamine B used for structure elucidation..…….....40

Table 3.2 Chromatographic and mass spectrometric information of metabolites of ceratamine A used for structure elucidation……..……..……44

Table 3.3 Relative abundances of phase I metabolites of the ceratamines after 60 min incubations with rat liver microsomes……...54

Table 3.4 Accurate mass determination results for proposed molecular formulas of metabolites of the ceratamines.……..55

Table 3.5 ^{1}H NMR Spectroscopic Data of ceratamine B, M4, and M6.……60

Table 4.1 Lipinski's rule characteristics of the ceratamines.…….75

Table 4.2 Control compounds used for metabolic stability assay in rat liver microsomes……...76

Table 4.3 Validation of metabolic stability assay with rat liver microsomes.……78

Table 4.4 Estimated clearance categories of the ceratamines……80

Table A1 Accurate mass determinations of major fragments of the ceratamines……95

LIST OF FIGURES

Figure 1.1 Ribbon diagram of the α-, β-tubulin heterodimer and the structure of a microtubule, consisting of 13 protofilaments wrapped around a hollow core. 3

Figure 1.2 Straight and curved conformations of the plus end of microtubules. 5

Figure 1.3 Reorganization of Microtubules during mitosis. 7

Figure 1.4 Structures of the vinca alkaloids vinblastine and vincristine.. 8

Figure 1.5 Paclitaxel binding site within β-tubulin. 9

Figure 1.6 Confocal images of MCF-7 cells treated with paclitaxel and vinblastine. 10

Figure 1.7 Structures of Marine Natural Products Ceratamine A and Ceratamine B. 13

Figure 1.8 Effect of Ceratamine A on mitotic cells.. 15

Figure 3.1 RP HPLC-UV chromatograms of 60 min rat microsomal incubations of the ceratamines.. 37

Figure 3.2 $[M+H]^+$ ion clusters and CID product ions of the ceratamines... 38

Figure 3.3 Neutral loss scans of the ceratamines... 39

Figure 3.4 $[M+H]^+$ ion cluster and CID product ions of M1... 41

Figure 3.5 $[M+H]^+$ ion cluster and CID product ions of M2.. 41

Figure 3.6 $[M+H]^+$ ion cluster and CID product ions of M3... 42

Figure 3.7 $[M+H]^+$ ion clusters and CID product ions of M4 and M6... 43

Figure 3.8 $[M+H]^+$ ion cluster of M9. 43

Figure 3.9 $[M+H]^+$ ion clusters of M10, M4, and M6... 46

Figure 3.10 CID product ions of M10 and M4.. 46

Figure 3.11 Comparison of retention times of ceratamine B and CB..... 47

Figure 3.12 $[M+H]^+$ ion cluster and CID product ions of M8... 48

Figure 3.13 $[M+H]^+$ ion clusters of M5, M7, and CB... 49

Figure 3.14 CID product ions of M5, M7, and CB..... 49

Figure 3.15 MRM analysis of metabolites of ceratamine A formed by rat liver microsomes.... 50

Figure 3.16 MRM analysis of metabolites of ceratamine B formed by rat liver microsomes..... 51

Figure 3.17 Proposed structures of the phase I metabolites of the ceratamines.... 52

Figure 3.18 RP-HPLC-UV chromatogram of a co-injection of 60 min rat microsomal incubations of ceratamine A and B..... 53

Figure 3.19 HPLC-UV chromatogram displaying optimized separation of metabolites of ceratamine B using a semi-preparative column..... 56

Figure 3.20 Effect of injection volume on separation of metabolites of ceratamine B using semi-preparative conditions..... 57

Figure 3.21 UV/Vis absorbance spectra of ceratamine B, M3, M4, and M6. 58

Figure 3.22 Proposed structures of two major phase I metabolites of ceratamine B formed by rat liver microsomes..... 61

Figure 4.1 Formation of metabolites of ceratamine A by rat liver microsomes.. 63

Figure 4.2 Formation of metabolites of ceratamine B in rat liver microsomes.. 64

Figure 4.3 RP-HPLC-UV chromatograms of incubations of ceratamine A with rat and human liver microsomes..... 65

Figure 4.4 $[M+H]^+$ ion cluster and CID product ions of M9 formed by human liver microsomes.. 66

Figure 4.5 $[M+H]^+$ ion cluster and CID product ions of M8 formed by human liver microsomes……67

Figure 4.6 $[M+H]^+$ ion clusters and CID product ions of M5 and M7.. 68

Figure 4.7 Formation of metabolites of ceratamine A in human liver microsomes.. 69

Figure 4.8 RP-HPLC-UV chromatograms of incubations of ceratamine B with rat and human liver microsomes.. 69

Figure 4.9 $[M+H]^+$ ion cluster and CID product ions of M1 formed by human liver microsomes.. 70

Figure 4.10 $[M+H]^+$ ion clusters and CID product ions of M4 and M6 formed by human liver microsomes.. 71

Figure 4.11 Formation of metabolites of ceratamine B in human liver microsomes.. 72

Figure 4.12 Species comparison of the metabolic profiles of the ceratamines in rat and human liver microsomes…..……73

Figure 4.13 Depletion profiles of control compounds used for the validation of the metabolic stability assay in rat liver microsomes……...77

Figure 4.14 Depletion profiles of control compounds used for the validation of the metabolic stability assay in human liver microsomes……79

Figure 5.1 Depletion profile of ceratamine B in human liver microsomes……..……82

Figure 5.2 Effect of total P450 content on the rate of formation of M2……..……..83

Figure 5.3 Effect of NADPH on depletion of ceratamine B in rat liver microsomes.……..…..84

Figure 5.4 Depletion of ceratamine B and formation of M3, M4, and M6 in human liver microsomes using optimized conditions……..……85

Figure 5.5 Effect of 1-aminobenzotriazole (ABT), on the formation of the major metabolites of ceratamine B in human liver microsomes ……86

Figure 5.6 Effect of NADPH on the formation of M6 in HLMs.. 87

Figure 5.7 Isozyme mapping of the formation of M3 and M4…….…89

Figure 5.8 Effect of ketoconazole on the formation of the major metabolites of ceratamine B in human liver microsomes.. 90

Figure A1 ^{1}H NMR spectrum of ceratamine B……..95

Figure A2 ^{1}H NMR spectrum of M4……...96

Figure A3 ^{1}H NMR spectrum of M6……....97

Figure A4 $[M+H]^+$ ion clusters and product ions of M10 formed by HLMs…….....97

Figure A5 $[M+H]^+$ ion clusters and product ions of M3 formed by HLMs…….98

ABBREVIATIONS

ABT	1-Aminobenzotriazole
CB	Ceratamine B formed as a metabolite from ceratamine A
GDP	Guanosine Diphosphate
GTP	Guanosine Triphosphate
HLMs	Human Liver Microsomes
HPLC	High Performance Liquid Chromatography
LC	Liquid Chromatography
LC-MS/MS	Liquid Chromatography-tandem Mass Spectrometry
M1, M2, etc.	Metabolite 1, Metabolite 2 etc…
MRM	Multiple Reaction Monitoring
MS/MS	Tandem Mass Spectrometry
NADPH	Nicotinamide adenine dinucleotide phosphate
QqQ	Triple Quadrupole Mass Spectrometry
QqTOF	Quadrupole-Time of Flight Mass Spectrometry
RLMs	Rat Liver Microsomes
RP-HPLC	Reversed Phase High Performance Liquid Chromatography

1.0 INTRODUCTION

1.1 MARINE NATURAL PRODUCTS IN DRUG DISCOVERY

Natural products have been an essential component of drug discovery and development for hundreds of years.[1] To date approximately 50% of drugs approved in the United States each year are or are derived from natural products.[1,2] Initial interest in natural products as sources of therapeutic agents centered around terrestrial species, which was mostly due to the ease of access to these plants and organisms. Many commonly used drugs including analgesics such as morphine and lidocaine, and antibiotics such as penicillin were discovered from terrestrial plants.[1,3]

Marine organisms were discovered as an additional source of biologically active natural products over 60 years ago.[4] These studies were limited, however, due to difficulty in accessing the majority of marine environments. Interest began to rapidly increase as technological advances allowed access to numerous deep sea species including marine bacteria, bryozoans, ascidians, and sponges, which were found to contain biologically active natural products.[4] Many of these products have unique structural features, such as large rings and macrocyclic structures, that have not been found within terrestrial organisms.[5] Another advantage of marine natural products is their potency. Marine organisms, especially invertebrates such as sponges, have little mobility and have developed self-defenses in order to survive. They, or their microbiological

inhabitants, are able to synthesize and release very potent toxins that offer protection from predators. Many of these toxins have been found to have activities that may have therapeutic use.[6]

In 2004, the United States Food and Drug Administration (FDA) approved the first drug derived from a marine source. Ziconotide (Prialt™), which was isolated from a cone snail, is a peptide that is used for the treatment of chronic pain.[3] Then, in 2007, the European Union approved trabectedin (Yondelis™) for use as an anti-cancer agent.[3] It is currently estimated that approximately 118 marine natural products are in preclinical trials and 22 are in clinical trials.[7]

1.2 ANTIMITOTIC NATURAL PRODUCTS

Marine environments have been found to be a rich source of natural products that display a wide variety of biological activities. A large number of compounds, especially those isolated from marine sponges, have been found to display antimitotic activity.[3] The mechanism of this activity includes the targeting of microtubules.[3,8]

Microtubules are one of three types of biological polymers found in eukaryotic cells.[9] The monomeric unit of microtubules is tubulin, which is a globular protein that consists of 12 α helicies, a 4 strand β-sheet and a 6 strand β-sheet.[10] Tubulin forms a heterodimer between α and β tubulin (Figure 1.1). Each dimer links together, forming a chain known as a protofilament. On average, 13 protofilaments attach due to lateral and longitudinal interactions to form a microtubule with a hollow core.[9]

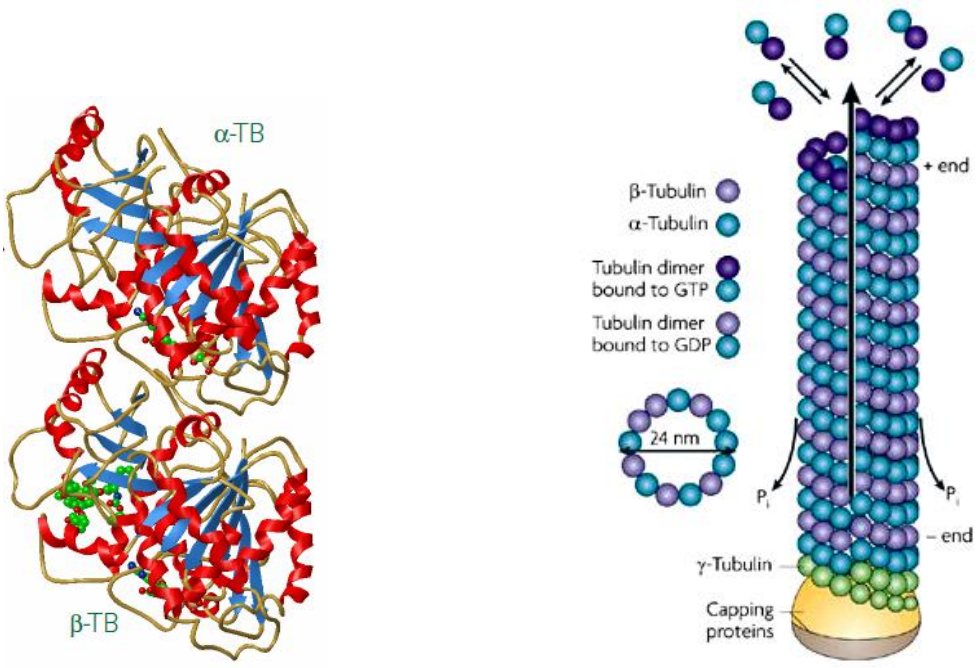

(A) (B)

Figure 1.1. (A) Ribbon diagram of the α-, β-tubulin heterodimer [Adapted by permission from Macmillan Publishers Ltd: Nogales *et* al., *Nature*, **1998**, *391*, 199-203.[10]]. (B) Structure of a microtubule, consisting of 13 protofilaments forming through lateral contacts a cylinder wrapping around a hollow core [9] [Adapted by permission from Macmillan Publishers Ltd: Conde, C. and Cáceres, A., *Nature Reviews Neuroscience*, **2009**, *10*, 319-322.[11]].

Microtubule formation begins at a cellular structure known as the microtubule organizing center. The major component of this center is the centrosome, which contains γ-tubulin, another globular protein that is responsible for the attachment of the first subunits of the microtubule.[9] The point of attachment is referred to as the minus end of the microtubule. The plus end grows away from the nucleus, towards the periphery of the cell.

Many biological assemblies behave as equilibrium polymers that are dependent mainly on the free concentration of monomers to dictate formation.[12] The gain or loss of tubulin subunits in microtubules occurs through a unique process known as dynamic instability, which is

independent of the free tubulin concentration. Microtubules are constantly gaining and losing tubulin subunits, and a single microtubule can even gain and lose tubulin simultaneously, a process known as treadmilling.[9,12] The ability to rapidly change from polymer growth to shortening is crucial for the different cellular functions of microtubules and varies throughout the cell cycle. This dynamicity is tightly controlled in many ways, which makes the formation of microtubules unique and far different from equilibrium polymers. The regulation of microtubule formation is not completely understood but it is thought to be majorly controlled by the hydrolysis of guanosine triphosphate (GTP) which may be triggered by the binding of microtubule associated proteins (MAPs).[12, 13]

Each tubulin heterodimer contains two nucleotide binding pockets, one within α-tubulin, and one within β-tubulin. These pockets are able to bind one molecule of GTP, which is required for tubulin polymerization. The GTP bound within α-tubulin is non-exchangeable; however, the β-tubulin bound GTP is exchangeable and is thought to play a major role in microtubule dynamics.[9, 12] The addition of each tubulin dimer to a microtubule results in the hydrolysis of GTP to GDP. The plus end of every microtubule consists of multiple exchanged GTP units, known as the GTP cap. This cap maintains the straight conformation of the plus end, which is needed in order for the addition of tubulin subunits.[9, 12] If the cap begins to be hydrolyzed to GDP, which occurs when GDP to GTP exchange is reduced, the plus end is no longer stabilized and a conformational change occurs forming a curved plus end (Figure 1.2). This curved conformation does not allow for additional tubulin subunits to bind and polymerization is stopped.

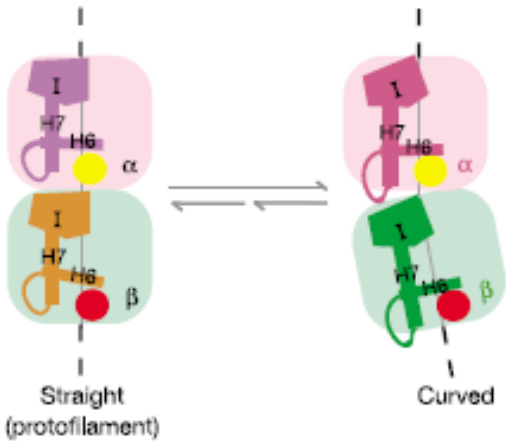

Figure 1.2. Straight and curved conformations of the plus end of microtubules [Adapted by permission from Macmillan Publishers Ltd: Ravelli *et* al., *Nature*, **2004**, *428*, 198-202.[14]].

It is not fully understood how GTP hydrolysis is triggered by the cell; however, it has been suggested that microtubule dynamics could be controlled through the binding of MAPs including MAP-1, MAP-2, MAP-4, tau, and even G-proteins.[9, 12, 13, 15] G-Proteins are involved in many cellular activities including extracellular signaling. Specifically, the α-subunit of G-proteins has been found to cause a microtubule catastrophe, which is the transition from polymer growth to disassembly.[15] The mechanism of this inhibition has been investigated and it has been proposed that the α-subunit can affect microtubule dynamics in two ways. First, the exchangeable GTP bound within β-tubulin can bind to the G-protein, leaving the microtubule without the necessary nucleotide. Second, the α-subunit can also activate the intrinsic GTPase activity of tubulin that normally is only active after multiple tubulin heterodimers have been incorporated into the polymer.[15]

The ability of the cell to control microtubule assembly and disassembly is essential for cell survival. Microtubules have numerous cellular functions.[9, 12] They are an important part of the cytoskeleton and help to provide structural support.[8] Many motor proteins, such as the

dyneins and the kinesins, are able to attach to microtubules and transport various components throughout the cell.[16] This had led to microtubules commonly being referred to as the 'highway' or 'railway' of the cell.[9] Perhaps the most important function of microtubules, for the field of cancer drug discovery, is their role in mitosis.[8] During this process, genetic information stored in chromosomes must be duplicated and transported to opposite ends of the cell before division occurs. This is accomplished by the mitotic spindle, which is dependent on microtubules for proper function.[16]

Prior to mitosis, the organization of microtubules drastically changes. The duplicated chromosomes are also accompanied by a duplicated centrosome which will act as a second site for microtubule formation.[9] Therefore, currently formed microtubules need to disassemble to allow for the mitotic spindle to be formed. The spindle consists of three types of microtubules, kinetochore, polar, and astral microtubules. Kinetochore microtubules are attached to the chromosomes and the centrosomes. Polar microtubules are attached to the centrosomes and grow towards each other to form an overlapping structure. Astral microtubules are also attached to the centrosomes, however they grow out into the periphery of the cell (Figure 1.3).[9] These microtubules are responsible for attaching the chromosomes to the spindle, stabilizing and transporting the spindle through the cell, and ensuring that the chromosomes are in the correct orientation for mitosis to occur.[8, 16] A high rate of dynamic instability is crucial for the spindle to function correctly; therefore, anything that can disrupt the dynamicity during this stage of the cell cycle will prevent the formation of the mitotic spindle which will result in mitotic arrest and, eventually, cell death.[16]

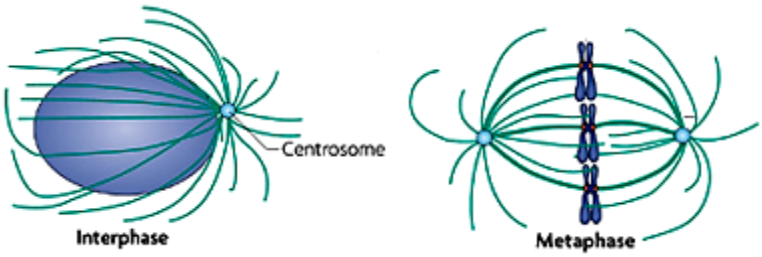

Figure 1.3. Reorganization of microtubules during mitosis [Adapted by permission from Macmillan Publishers Ltd: Walczak *et* al., *Nature Reviews Molecular Cell Biology*, **2010**, *11*, 91-102.[17]].

Small molecules that are able to interrupt the dynamicity of microtubules are often referred to as microtubule perturbers or perturbagens. There are three major small molecule binding sites on tubulin: the colchicine, vinca alkaloid, and taxol sites.[13, 18, 19] Each site is named after the major microtubule perturbagen that interacts with tubulin via this site.

Colchicine is a small molecule that was isolated from the plant, *Colchicum autumnale* (Figure 1.4).[20] The polymerization of purified tubulin is prevented in the presence of colchicine *in vitro*, therefore it is considered a microtubule destabilizer. This inhibitory activity is due to colchicine's ability to bind to tubulin.[14] The binding site is at the intradimer contact region, located between α-1 and β-1 tubulin.

Colchicine preferentially binds to free tubulin subunits and not directly to the microtubule. Once the colchicine-tubulin complex has formed, it can add to the plus end of the microtubule. This bound complex can no longer remain in the straight protofilament conformation, due to steric hinderance between colchicine and several amino acid residues of α-tubulin.[14] The loss of stability of the plus end prevents the addition of any tubulin subunits and eventually results in disassembly. The inhibition of tubulin polymerization interrupts the dynamic instability that is crucial for many cellular functions, especially mitosis. Colchicine-

exposed cells cannot properly form the mitotic spindle and the result is mitotic arrest and cell death.[14]

Vinblastine is a natural product isolated from the periwinkle, *Catharanthus roseus*.[21] It is a member of the vinca alkaloid family, which also includes vincristine (Figure 1.4). Numerous analogues of vinblastine and vincristine have been synthesized including vindesine, vinorelbine, and vinflunine.[21]

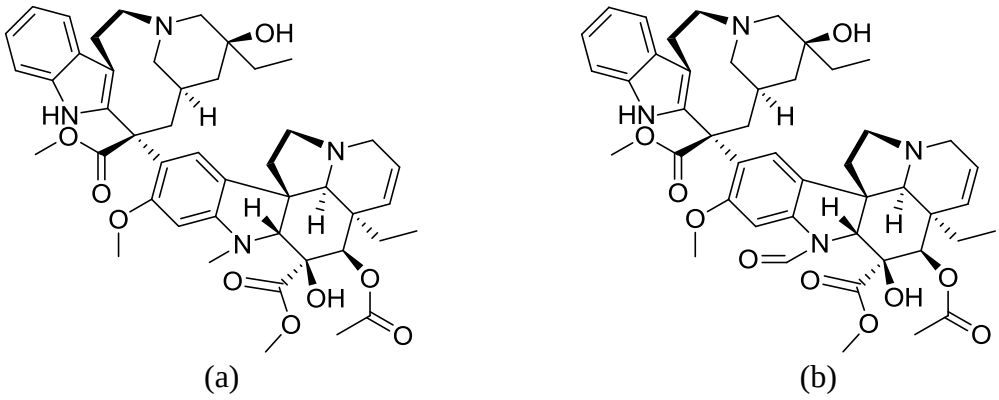

Figure 1.4. Structures of the vinca alkaloids (a) vinblastine, (b) vincristine.

The vinca alkaloids are also microtubule destabilizers; however, they have a different mode of action than colchicine. The vinblastine binding site is located in close proximity to the GTP binding site within β-tubulin. The position of this nucleotide within tubulin is an exchangeable site which is thought to be essential to the regulation of microtubule dynamics. Once vinblastine is bound to tubulin, this GTP site is blocked which does not allow for any GDP-GTP exchange to occur. Without this exchange, the GTP cap at the plus end of the microtubule is diminished, leading to a conformational change from straight protofilaments to a curved plus end.[18] The curved conformation is not conducive to binding of tubulin subunits;

therefore, polymerization is ceased and disassembly will eventually occur. Another difference from colchicine is that high concentrations of vinblastine cause alternate, non-functional structures of microtubules to form.[22]

Paclitaxel (Taxol®) is a member of the taxanes, a group of natural products isolated originally from the Pacific Yew tree, *Taxus brevifolia*.[21] Until their discovery, the majority of known microtubule perturbagens were destabilizers of tubulin polymerization. The taxanes are however, able to disrupt microtubule dynamics through the stabilization of tubulin protofilaments.[19] The binding site of paclitaxel is located within β-tubulin (Figure 1.5). The presence of paclitaxel maintains the ideal straight conformation, most likely through interaction with the M-loop, which allows for polymerization to continue.[23]

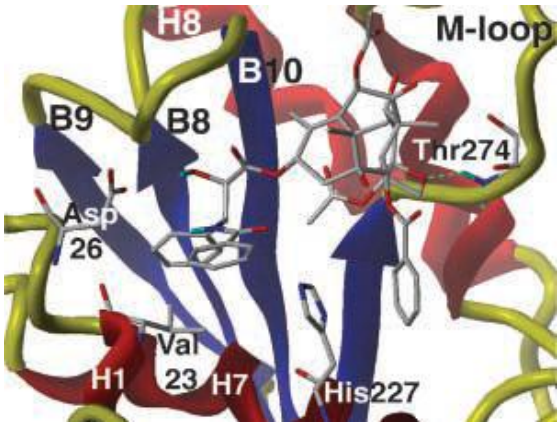

Figure 1.5. Paclitaxel binding site within β-tubulin [Adapted from *Molecular Cancer Therapeutics*, 2006, *5*, 270-278, Hari *et* al., Paclitaxel-resistant cells have a mutation in the paclitaxel-binding region of β-tubulin (Asp26Glu) and less stable microtubules, with permission from AACR[23]].

The effect of these various microtubule perturbagens on microtubule formation can actually be visualized by microscopy (Figure 1.6). By differential staining of the DNA and microtubules, the differences between destabilizers and stabilizers can be appreciated. The

untreated cells contain a complex network of microtubules which provide structural support. Cells treated with the microtubule stabilizer paclitaxel have large bunches of long microtubules that surround the nucleus of the cell. The microtubule destabilizer, vinblastine, results in a large amount of short microtubules.[24] Although the mechanism of each drug is different, the same result is achieved--mitotic arrest that will lead to cell death.[24]

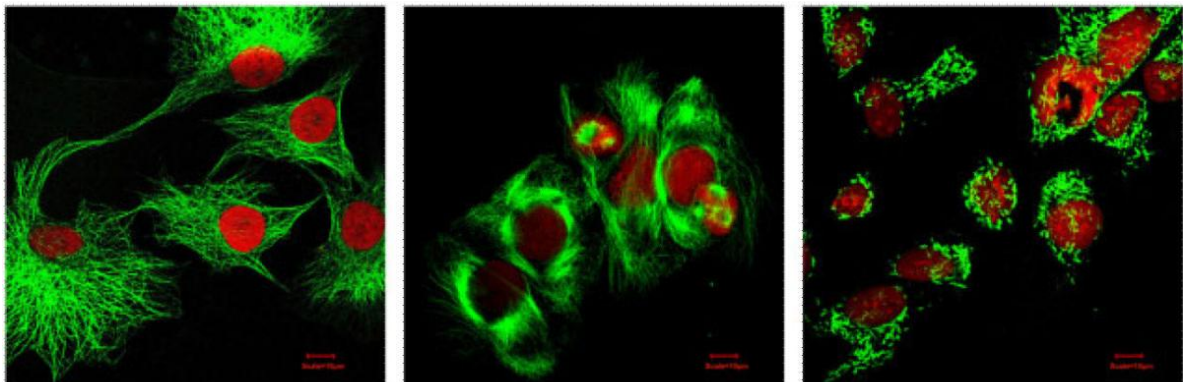

(A) (B) (C)

Figure 1.6. Confocal images of MCF-7 cells' chromatin (red) and microtubules (green) in: (A) untreated control cells; (B) cells treated with paclitaxel; (C) cells treated with vinblastine [Adapted with permission © 2011 Wiley Periodicals, Inc. Med Res Rev, 31, No. 3, 443-481, 2011.[24]].

1.3 CLINICAL SIGNIFICANCE OF MICROTUBULE PERTURBAGENS

Traditionally, microtubule perturbagens have been of great interest to the field of cancer drug discovery. Although their antimitotic activity is not selective for cancer cells, when dosed appropriately, microtubule perturbagens can be especially effective in highly proliferative cells.[25] This observation was supported with the approval and use of Taxol® in the treatment of various cancers. Due to its potency, paclitaxel is considered the gold standard microtubule stabilizer.[26] Although efficacious, the development of resistance remains an immense challenge. Therefore,

the discovery of novel microtubule perturbagens, especially those with a different mechanism, i.e. a different binding site, is of importance.

Two mechanisms of such resistance have been proposed. A primary cause, initially identified within *in vitro* methods, are mutations within β-tubulin. In fact, two taxol-resistant human ovarian carcinoma cell lines have been reported, 1A9PTX10 and 1A9PTX22. These cells have point mutations within the taxol binding site that result in a 24-fold resistance to paclitaxel treatment.[26] Recently, it has been observed that three mutations identified in various human cancers: A185T, A248V, and R306C, also can cause a loss of sensitivity to paclitaxel. These mutations are not in the taxol binding site within β-tubulin, but have been found to affect microtubule stability, a characteristic that may be able to overcome the effects of taxol.[27] Finally, paclitaxel is also a substrate for P-glycoprotein, an efflux pump commonly involved in the development of multidrug resistance due to its role in the transport of various hydrophobic compounds out of cells.[28]

In addition to anticancer drug development, it has also been suggested that microtubule stabilizers may be effective in the treatment of tauopathies, various neurodegenerative diseases including Alzheimer's disease.[29] As previously discussed, microtubules play an important role in transport throughout the cell. Specifically within neurons, the motor proteins dynein and kinesin attach to microtubules in order to ensure proper axonal transport. Tau is a protein present within neurons. It has been found to display endogenous microtubule stabilizing activity. Once bound to a microtubule, tau prevents its disassembly, allowing the cellular 'railway' to remain intact. In the development of tauopathies, this protein becomes hyper-phosphorylated, resulting in a loss of binding affinity toward microtubules. With the loss of stabilization, the microtubule is now able to disassemble, preventing the proper transport of axons, an observation noticed in many

neurodegenerative diseases.[29] Therefore, treating with small molecule microtubule stabilizers may be effective in overcoming the loss of the endogenous stabilization activity of tau. One of the greatest challenges in testing this hypothesis is the identification of small molecules that are able to cross the blood-brain barrier.[29]

1.4 CERATAMINES A AND B

Due to the success of microtubule perturbagens as anti-cancer agents, interest began to increase in identifying new antimitotic natural products. To aid in this identification, high-throughput cell based assays have been developed.[30] Such assays involve three different techniques to identify anti-mitotic activity. These techniques include visualization by microscopy, enzyme-linked immunosorbent assay (ELISA), and enzyme-linked immunocytochemistry (ELICA). The use of ELISA requires an antibody-antigen interaction that is specific for the activity of interest and will promote a measureable response. The monoclonal antibody TG-3 can be used due to its specificity for mitotic cells.[30] This antibody only reacts with phosphorylated nucleolin, which is formed upon mitosis. After the antigens and antibodies are allowed to react, an antibody which is conjugated to horseradish peroxidase (HRP) can be added which will result in a measureable colorimetric response upon the addition of a proper HRP substrate.[30]

The ELICA assay was developed based on the same principles as ELISA. Instead of preparing titer plates with fixed antibodies, the cells can be fixed to the plate. This can allow for the TG-3 monoclonal antibody and HRP-conjugated antibody to be added at the same time. The ELICA assay involves a simpler procedure which contains fewer steps due to the minimized number of washes needed when using fixed cells instead of mixed antibodies.[30]

The high throughput anti-mitotic assay was used to screen 24,000 extracts of different species ranging from marine invertebrates to terrestrial plants. A total of 119 extracts were found to contain antimitotically active natural products.[30] One of these extracts was obtained from the marine sponge *Pseudoceratina* sp. recovered in Papua, New Guinea.[31] Bioassay-guided fractionation was used to isolate the specific natural products which are responsible for the desired antimitotic activity. This process involves fractionating the crude extract using a separation technique such as high performance liquid chromatography (HPLC). Each fraction is tested for the desired activity and the purity of the active fractions is tested by techniques such as liquid chromatography-mass spectrometry (LC-MS). Once a pure natural product has been isolated, structure elucidation is achieved using many spectroscopic techniques such as fourier transform infrared (FTIR), UV/Vis, and nuclear magnetic resonance (NMR) spectroscopy.[32]

Ceratamines A and B are heterocyclic alkaloids that were isolated from *Pseudoceratina* sp. (Figure 1.7).[31] They have IC_{50} values of 15 µM and 25 µM, respectively for antimitotic activity.[31]

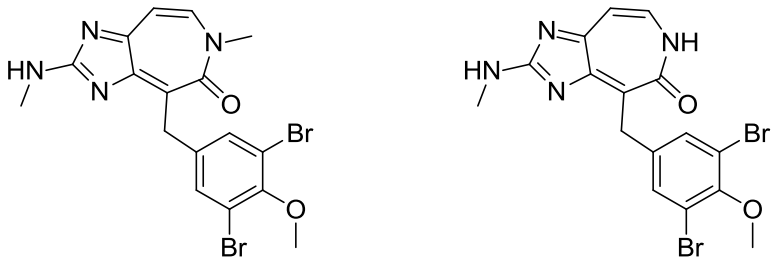

(A) (B)

Figure 1.7. Structures of the marine natural products (A) ceratamine A and (B) ceratamine B.

Since a large majority of antimitotic agents interact with microtubules, numerous tubulin polymerization assays have been performed to determine if the ceratamines were also

microtubule perturbers.[31, 33] The potential of the ceratamines to inhibit tubulin polymerization was tested by incubating 3 mg/mL of purified bovine tubulin with 100 μM of ceratamine A or B. GTP was also included in the reaction mixture. The temperature was increased from 0 to 37°C where, in the absence of an inhibitor, purified tubulin polymerizes in the presence of GTP. Tubulin polymerization can be determined by monitoring the turbidity of the solution at 340 or 350 nm.[34] No significant difference in the amount of tubulin polymerization was noticed between the ceratamine reaction mixture and vehicle controls; therefore, the ceratamines are not inhibitors of tubulin assembly.[31]

The ability of the ceratamines to stabilize microtubules was investigated by incubation with 1 mg/mL of purified bovine tubulin. Polymerization occurred in the presence of either of the ceratamines, suggesting their mechanism of antimitotic activity is by microtubule stabilization since low concentrations of purified tubulin will not polymerize spontaneously. Their ability to stabilize microtubules is less than that of paclitaxel.[31]

Cells treated with ceratamine A were unable to properly form the mitotic spindle, therefore chromosome segregation was not achieved (Figure 1.8).[33] The stabilization of microtubule formation causes a disruption in the dynamicity of microtubules that prevents the proper formation and function of the mitotic spindle, leading to mitotic arrest.[33]

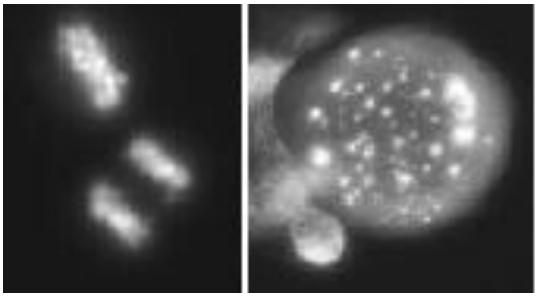

(A) (B)

Figure 1.8. Effect of ceratamine A on chromatin in mitotic cells, (A) untreated cells showing chromosomes congressed to the mitotic plate (upper left) and proper anaphase showing evenly segregating chromosomes (lower right), and (B) cell treated with 20 μM ceratamine A showing uncongressed and punctuate chromatin [Adapted from *Cancer Research,* 2005, 65, 3040-3043, Karjala *et* al., Ceratamines, Structurally Simple Microtubule-Stabilizing Antimitotic Agents with Unusual Cellular Effects, with permission from AACR[33]].

Although the ceratamines are not as potent as paclitaxel, which has an IC_{50} of 1.5 nM within the antimitotic assay, the discovery of this novel class of microtubule stabilizers is due to their significant structural differences compared to all known microtubule perturbagens.[31, 33] Although they contain an atypical imidazoazepinone moiety, they are structurally simple, allowing for efficient total synthesis.[35] They are also the only known microtubule perturbagens that are achiral.

The exact microtubule/tubulin binding site of the ceratamines has not been identified, but it has been determined through a competitive binding assay that they do not bind at the same site as paclitaxel.[33] The uniqueness of their structures and the lack of competition for the paclitaxel binding site also gives the ceratamines great potential as anticancer agents, particularly for possible use in combination therapies to overcome the development of drug resistance, a major limitation of Taxol® treatment. Although the ability of the ceratamines to cross the blood-brain

barrier has not been reported, due to their simple structures, they may be ideal candidates to test the hypothesis that microtubules may be effective in the treatment of tauopathies.

1.5 PROJECT GOALS

The primary focus of all reported studies on the ceratamines has been on establishing biological activity.[31, 33] This project represents the first pre-clinical studies of this novel class of microtubule stabilizers. The specific emphasis is on performing certain pharmacokinetic studies, in order to begin to understand the effect the human body will have on these potential drugs. In particular, the phase I metabolism of each compound has been investigated.

My first goals is to identify the phase I metabolites of each of the ceratamines formed by rat and human *in vitro* enzyme systems. This involves comparing the overall metabolic profile including the number of total metabolites formed, the structures of each metabolite, and their relative abundances. Second, I want to determine the stability of each compound within rat and human *in vitro* enzyme systems. My final goal is to determine which drug metabolizing enzymes are involved in the formation of the major phase I metabolites of ceratamine B in a human *in vitro* enzyme system.

1.6 METABOLISM

1.6.1 Introduction to xenobiotic metabolism

Xenobiotic (e.g. drug) metabolism is a complex enzymatic process with the purpose of eliminating exogenous species from the body.[36- 38] This goal is obtained by chemically modifying the substance to decrease lipophilicity, resulting in easier excretion.[36, 37]

There are numerous types of metabolic reactions which are typically divided into two phases. Phase I metabolism involves simple functional changes resulting from oxidation, such as hydroxylations, demethylations, reductions, and hydrolysis.[37, 39] If the polarity of a xenobiotic can be significantly increased by the addition or removal of a simple functional group, then phase I metabolism will be sufficient. If these simple changes will not ease renal excretion, then the purpose of phase I is to create a reactive site that will allow phase II reactions to occur.[40]

Phase I reactions are majorly catalyzed by a superfamily of enzymes known as cytochromes P450.[36-39] The majority of P450s are found within the liver; however, metabolism can occur in various locations throughout the body including the kidney, lungs, and blood.[38] Specifically, P450s are attached to the inside membrane of the smooth endoplasmic reticulum. The lipophilicity of this environment attracts most drugs, allowing for efficient transport to P450s.[37]

P450s are of extreme importance as they are responsible for more than 75% of xenobiotic metabolism.[37, 40] There are 57 different human P450s, which are divided into 18 families and further divided into subfamilies. These divisions are based on the homology of their sequences. P450s belonging to the same family have 40% similarity, subfamilies have 55% similarity, and an individual isoform from the same subfamily will only differ by 3%.[37] Only 15 P450s are

involved in drug metabolism, with CYP3A4 (belonging to family 3 and subfamily A) being the most commonly involved P450 in drug metabolism (Table 1.1). There are many suggestions as to why CYP3A4 is thought to be so actively involved. One explanation is that it is the most highly expressed, particularly in the small intestine, of the P450s in humans; therefore it would be expected to be involved in many reactions. A second explanation is that CYP3A4 is the most flexible P450, which could allow for a larger number of substrates to bind.[37]

The three dimensional structure of P450s is very similar to a hand. Near the center of the "palm" is a heme group, which contains the catalytically active iron atom, named protoporphyrin IX. This is the active site of the P450. The remainder of the structure can move similar to fingers, therefore the flexibility of these domains dictates the ability of substrate binding.[37]

Table 1.1. Human cytochrome P450 isoforms involved in xenobiotic metabolism.[37]

CYP 1 Family	CYP 2 Family	CYP 3 Family
CYP1A1	CYP2A6	CYP3A4
CYP1A2	CYP2A13	CYP3A5
CYP1B1	CYP2B6	CYP3A7
	CYP2C8	
	CYP2C9	
	CYP2C18	
	CYP2C19	
	CYP2D6	
	CYP2E1	

P450s require reduction-oxidation (redox) partners to properly function. The most important partner is P450 oxidoreductase (POR). This flavoprotein complex consists of flavin adenine dinucleotide (FAD) and flavin mononucleotide (FMN). The purpose of this complex is to pass two electrons to the P450 to allow metabolic reactions to occur. This electron flow is initiated by one molecule of nicotinamide adenine dinucleotide phosphate (NADPH); therefore, NADPH is a cofactor required for P450-mediated metabolism. NADPH reduces FAD to form

$FADH_2$. $FADH_2$ reduces FMN to form $FMNH_2$, which passes two electrons to the nearby P450. Other redox partners have been identified, such as cytochrome b_5; however, their function is not fully understood.[37]

Cytochromes P450 mainly behave as monooxygenases; therefore, many P450-mediated metabolites include an oxygen containing functional group such as an alcohol or epoxide. Common phase I reactions include aromatic hydroxylations, *N*-dealkylations, *O*-dealkylations, deaminations, and dehalogenations.[37, 35]

Phase II metabolism involves the formation of conjugates with molecules such as glucuronic acid, sulfonates, glutathione, methyl groups, and amino acids. Again the purpose is to increase the hydrophilicity of the xenobiotic. If a conjugate is required to achieve a desirable polarity increase then it generally occurs after a phase I reaction, however it is possible for a phase II reaction to occur initially.[37-40]

1.6.2 Metabolism studies *in vitro*

The tedious nature of the drug discovery process is essential to ensuring the availability of only safe and effective drugs, however this results in a high attrition rate, leading to tremendous losses in both time and expenses. Many drugs fail due to toxicity seen in clinical trials (humans) that was not apparent during pre-clinical trials (animals).[39] It is possible that some toxicity may be a result of the formation of toxic metabolites; therefore, the addition of thorough pre-clinical metabolism studies can be beneficial in identifying toxicity due to biotransformation. The formation of a toxic metabolite can be avoided by slightly changing the structure of the lead compound so that the toxic metabolic pathway cannot occur. This is much easier at this early stage.[39]

The simple approach to begin to study the metabolism of a potential drug candidate is through the use of *in vitro* methods. All *in vitro* reaction mixtures must contain an enzyme system, appropriate cofactors to ensure activity, a proper buffering system, and the drug of interest. Although more simple than *in vivo* animal models, the use of human cells or tissue shows a higher *in vitro*-to-*in vivo* correlation within humans.[41] This is desirable, because it reduces the risk that a potential drug candidate will show unexpected toxicity within clinical trials.

Enzyme system choice is dependent on the overall goal of the experiment. Factors to consider include what phase of metabolism is the primary focus, the cellular location of the enzymes of interest, the specific population to be studied (e.g., children), species of interest, etc. Typically, *in vitro* studies begin with understanding the phase I metabolic reactions that occur, which requires an enzyme system containing cytochromes P450. Liver microsomes, which are obtained through differential centrifugation of homogenated liver tissue, are a rich source of P450s.[37, 41] Microsomes also contain uridine diphosphoglucuronosyl transferase (UGT), a major phase II enzyme that is responsible for the formation of glucuronyl conjugates. UGTs require uridine diphosphoglucuronic acid (UDGPA) to function; therefore, if only phase I P450-mediated processes are of interest, this can be controlled by only adding NADPH. Liver microsomes are commercially available and are typically "pooled" samples, meaning they were obtained from a large amount of donors, usually more than 20. Using pooled liver microsomes allows for a reasonable estimation of metabolism across a population. The use of an individual donor gives rise to the real risk that the results may be based on an abnormal metabolizer, either sensitive or insensitive, and does not reflect the true average of a population. Also, specialty

pools are available if a specific population is of interest, such as gender-specific pools, age-specific pools, or behavior-specific pools (smoker, etc.).[41]

The advantages of using liver microsomes include their commercial availability, their stability (enzyme activity can last for years if stored at −80°C), and the simple sample preparation. The major disadvantage of using microsomes is the incomplete metabolic profile obtained. Microsomes are generally only useful for the study of phase I metabolism. The drug has very easy access to P450s and there are no other enzymes competing for the substrate. Although this system may have a lower *in vitro*-to-*in vivo* correlation in comparison to other systems, it is a great starting point.[41]

Other enzyme systems can also be obtained using differential centrifugation of liver tissues. These include the cytosol and S9 fractions. Although the major phase II metabolizing enzyme, UGT, is found within the microsomal fraction, the majority of phase II enzymes are located within the cytosol. These include *N*-acetyl transferase (NAT), glutathione *S*-transferase (GST), thiopurine methyl transferase (TPMT), and sulfotransferase. Therefore, if understanding and identifying conjugated phase II metabolites is desired, the most efficient system would be the S9 fraction. This system contains both P450s (phase I) and the cytosolic phase II enzymes.[41]

In order to achieve higher *in vitro*-to-*in vivo* correlation, the use of human hepatocytes is recommended. Hepatocytes are cells that can be isolated from the liver. Unlike microsomes or other fractions collected by differential centrifugation, hepatocytes still contain active regulatory pathways. This allows all phases of metabolism to occur and also is affected by influences such as enzyme induction and the ability of the xenobiotic to enter the cell (since the membrane is still intact). The major disadvantage of this system is the short lifetime of the hepatocytes.[41]

The highest correlation with *in vivo* metabolism can be obtained using precision cut liver slices or *in situ* liver perfusion. These systems still contain drug transport pathways, enzyme regulatory pathways, and cell-cell interactions. Although liver slices are the closest system to actual human metabolism, they are only viable for 5 days after slicing.[41]

Besides the identification of phase I and phase II metabolites, *in vitro* systems can be used to obtain other important information. This information includes simple species comparisons, P450 isoform identification, P450 induction/inhibition prediction, and biological activity and toxicity testing of metabolites.[41, 42]

Phase I species comparisons can be performed using different types of liver microsomes, for example rat vs. human. This could help to predict the *in vitro*-to-*in vivo* correlation between the metabolism in rats and humans. If the metabolic profile is similar between the two species, then *in vivo* results obtained from rats may be beneficial in predicting what to expect during clinical trials.

Identification of the specific P450 isoforms responsible for metabolite formation is very important in predicting the risk of drug-drug interactions. If the drug is rapidly metabolized by CYP3A4, then the consumption of another drug, which may be an inhibitor or inducer of CYP3A4, will change the bioavailability of the original drug. The presence of an inducer could result in a loss of efficacy, while an inhibitor may lead to an increase in toxicity. *In vitro* systems can also be used to determine if the drug of interest itself acts as an inducer or inhibitor of a certain P450 isoform.[41]

Finally, large scale *in vitro* metabolism reactions can be performed so as to allow for a substantial amount of metabolite(s) to be isolated. These metabolites can be tested for potential biological activities and toxicities. This can help to identify if the drug is acting as a pro-drug,

meaning it is metabolized to the active form, or if it is being negatively bioactivated, meaning it is metabolized to a toxic form.[41] Performing this evaluation at such an early stage in the drug discovery process could allow for small structural changes to be implemented within the drug that could increase activity or prevent a toxic metabolite from being formed. This could save countless hours and dollars for the future.

2.0 EXPERIMENTAL

2.1 MATERIALS

Ceratamines A and B were prepared by total synthesis.[35] Pooled Sprague-Dawley rat liver microsomes (20 mg/mL protein content, 0.728 nmol P450/mg protein) and pooled human liver microsomes (20 mg/mL protein content, 0.258 nmol P450/mg protein) were purchased from Invitrogen (Grand Island, NY). Metoprolol tartrate, propranolol hydrochloride, verapamil hydrochloride, β-nicotinamide adenine dinucleotide phosphate reduced tetra(cyclohexyl ammonium) salt, and ammonium acetate were purchased from Sigma-Aldrich (St. Louis, MO). Warfarin, Optima® LC/MS grade methanol, Optima® LC/MS grade water, Optima® LC/MS grade acetonitrile, ketoconazole, and dimethyl sulfoxide were purchased from Fisher Scientific (Pittsburgh, PA). Milli-Q H_2O was purified by Millipore Academic Milli-Q Water Purification System. CYP1A2, CYP2C8, CYP2C9, CYP2C18, CYP2C19, CYP2D6, CYP2E1, CYP3A4, and CYP3A5 (Bactosomes) obtained from *Escherichia coli* expressed recombinant enzymes were purchased from Xenotech (Lenexa, KS).

2.2 METHODS

2.2.1 Microsomal incubations

Incubation mixtures contained a final drug concentration of 10 µM, a final microsomal protein concentration of 0.3 mg/mL, and a final concentration of NADPH of 1 mM in 100 mM ammonium acetate buffer, pH 7.4. Reactions were initiated by the addition of NADPH and were incubated in a water bath at 37°C. Reactions were stopped by the addition of one volume of ice cold methanol. Samples and controls were placed on ice for approximately five minutes and were then centrifuged for ten minutes at 4500 rpm. The supernatant was collected and stored at −20°C until LC-MS/MS analysis. Two types of control incubations were also performed. These incubations contained microsomal protein previously inactivated by heating at 45°C for 30 min or microsomal protein that had been boiled for 6 min.

2.2.2 Large scale microsomal incubations

Incubation mixtures contained a final drug concentration of 50 µM and a final microsomal protein concentration of 2 mg/mL in 100 mM ammonium acetate buffer, pH 7.4. Total incubation volume was 5 mL. Reactions were initiated by the addition of NADPH. Cofactor was added every 15 min, maintaining a final concentration of 1 mM. Reactions were incubated in a water bath at 37°C for 1 h. Following incubation, reactions were stopped by the addition of one volume of ice cold methanol. Samples were placed on ice for approximately five minutes and were then centrifuged for 20 minutes at 4500 rpm. The supernatant was collected and stored at −20°C until isolation. A total of eight large scale reactions were performed.

2.2.3 Species comparison

Reaction mixtures contained final concentrations of 10 µM drug (ceratamine A or B), 0.3 mg/mL rat or human liver microsomes, and 1 mM NADPH in 100 mM ammonium acetate, pH 7.4. Controls were prepared using microsomes that were boiled for 6 min prior to incubation. Neat standards were prepared in ammonium acetate buffer. Reactions were initiated upon the addition of NADPH. Incubations were performed in a water bath at 37°C. Aliquots were removed at various time points (0, 15, 30, 45, and 60 min). Reactions were terminated upon the addition of one volume of ice cold MeOH. Following an approximately 5 min incubation on ice, reaction mixtures were centrifuged for ten min at 4500 rpm. Supernatants were collected and stored at −20°C until analysis. All samples and controls were performed in triplicate.

2.2.4 Metabolic stability assay

Reaction mixtures contained final concentrations of 1µM drug, 1 mg/mL (0.047 nmol P450/ mg protein) rat liver microsomes or 0.047 nmol P450/mg protein human liver microsomes, and 1 mM NADPH in a 100 mM ammonium acetate buffer at pH 7.4. Controls were prepared with microsomes that had been boiled for 6 min prior to incubation. Neat standards were prepared in ammonium acetate buffer. Reactions were initiated upon the addition of NADPH. Incubations were performed at 37°C for 30 min. Reactions were terminated by the addition of one volume of ice cold methanol. Following a 5 min incubation on ice, samples were centrifuged for ten min at 4500 rpm. Supernatants were collected and stored at −20°C prior to LC-MS/MS analysis. All samples and controls were performed in triplicate.

2.2.5 Incubations of ceratamine B with 1-aminobenzotriazole

Incubations were performed in a similar manner as previously described. Reaction mixtures contained final concentrations of 10 µM ceratamine B, 0.047 nmol P450/mg protein human liver microsomes in 100 mM ammonium acetate buffer, pH 7.4. A final concentration of 1 mM NADPH was utilized, however two additions of co-factor were performed at t=0 and t=15 min. For non-specific cytochromes P450 inhibition samples, 1-ABT (500 µM) was pre-incubated with human liver microsomes for 15 min at 37°C prior to addition of ceratamine B. Samples without any inhibitor were prepared for comparison. Boiled microsomes were used as a chemical stability control.

2.2.6 Incubations of ceratamine B with recombinant P450 isoforms

Incubations were performed in a similar manner as previously described. Reaction mixtures contained final concentrations of 10 µM ceratamine B and 1 mM NADPH in 100 mM ammonium acetate buffer, pH 7.4. Recombinant P450 concentrations were chosen according to the vendor. Reactions were initiated by the addition of NADPH. Following a 30 min incubation at 37 °C, reactions were terminated with the addition of one volume of ice cold MeOH. Samples were incubated on ice for approximately 5 min, centrifuged for 10 min at 4500 rpm, and stored at −20 °C prior to analysis.

2.2.7 Incubations of ceratamine B with a small molecule inhibitor of P450 isoforms

Incubations were performed in a similar manner as previously described. Reaction mixtures contained final concentrations of 10 µM ceratamine B, 1 µM ketoconazole, 0.047 nmol P450/mg protein human liver microsomes in 100 mM ammonium acetate buffer, pH 7.4. A final concentration of 1 mM NADPH was utilized, however two additions of co-factor were performed at t=0 and t=15 min. Samples without any inhibitor were prepared for comparison. Boiled microsomes were used as a chemical stability control.

2.3 ANALYSIS

2.3.1 HPLC-UV analysis

A Shimadzu Prominence HPLC coupled with a UV detector (Shimadzu Scientific Instruments, Columbia, MD) was used to determine the metabolic profiles of the ceratamines in rat and human liver microsomes and for P450 phenotyping of the major metabolites of ceratamine B. Separations were achieved using a ThermoFisher Beta Basic C_{18} column (150 x 2.1 mm, 5 µm particle diameter) (Fisher Scientific, Pittsburgh PA). Mobile phase A was H_2O containing 0.1% acetic acid. Mobile phase B was acetonitrile. A 25 µL injection volume was used for the species comparison experiment, while a 50 µL injection volume was utilized for the inhibition studies. The flow rate was 0.2 mL/min. UV analysis was performed using a wavelength of 350 nm. Separation of ceratamine metabolites was achieved using the following mobile phase gradient: 3 min hold at 15% B, increase to 17% B over 1 min, 18 min hold at 17% B, increase to 27% B

over 1 min, 4 min hold at 27% B, increase to 35% B over 2 min, 11 min hold at 35% B, decrease to 15% B over 2 min, 3 min hold at 15% B.

2.3.2 LC-MS/MS analysis

2.3.2.1 LC-triple quadrupole (QqQ) analysis

A Shimadzu Prominence HPLC equipped with a UV detector and coupled to an API 2000 triple quadrupole mass spectrometer with a turboion spray source (Applied Biosystems/MDS Sciex, Foster City, CA) was used to monitor metabolites of the ceratamines. Separations were achieved using a ThermoFisher C18 column (150 x 2.1 mm, 5 µM particle diameter). Mobile phase A was H_2O containing 0.1% acetic acid. Mobile phase B was CH_3CN.

The mobile phase gradient used for the separation of ceratamine A metabolites was as follows: 3 min hold at 15% CH_3CN, increase to 19% CH_3CN over 1 min, 7 min hold at 19% CH_3CN, increase to 27% CH_3CN over 2 min, 2 min hold at 27% CH_3CN, increase to 33% CH_3CN over 1 min, 10 min hold at 33% CH_3CN, decrease to 15% CH_3CN over 2 min, 7 min hold at 15% CH_3CN.

The mobile phase gradient used for the separation of ceratamine B metabolites was as follows: 1 min hold at 15% CH_3CN, increase to 50% CH_3CN over 3 min, 2 min hold at 50% CH_3CN, decrease to 15% CH_3CN over 2 min, 2 min hold at 15% CH_3CN.

Ideal MS parameters were determined by infusion of each compound. For metabolites of ceratamine A: IonSpray voltage was 5500 V, source temperature was 425 °C, declustering potential was 80 V, and focusing potential was 400 V. A collision energy of 50 (arbitrary units) was used for all metabolites of ceratamine A.

For metabolites of ceratamine B: IonSpray voltage was 5300 V, source temperature was

425 °C, declustering potential was 26 V, and focusing potential was 370 V. A collision energy of 37 (arbitrary units) was used for all metabolites of ceratamine B.

For the metabolic stability assay, MS parameters were optimized via infusion of each control compound. An isocratic mobile phase gradient of 50% mobile phase B. Tables 2.1-2.4 displays the optimized parameters for each compound.

Table 2.1. MS-MS source parameters used for the analysis of the ceratamines and the metabolic stability control compounds. Optimal conditions were determined by infusion.

Compound	$[M+H]^+$ (*m/z*)	Product Ion (*m/z*)	Source Temperature (°C)	IonSpray Voltage (V)
Ceratamine A	468.896	203.1	425	5300
	468.896	161.9	425	5300
Ceratamine B	454.852	189.0	425	5300
	454.852	134.1	425	5300
Metoprolol	268.168	116.0	425	5300
	268.168	74.0	425	5300
Nicardipine	480.036	315.0	425	4500
	480.036	91.0	425	4500
Propranolol	260.1	116.2	425	5300
	260.1	183.2	425	5300
Verapamil	455.238	165.0	400	5300
	455.238	150.1	400	5300
Warfarin	309.059	163.2	425	5300
	309.059	250.9	425	5300

Table 2.2. Additional MS-MS source parameters used for the analysis of the ceratamines and the metabolic stability control compounds. Optimal conditions were determined by infusion.

Compound	Nebulizer Gas (psi)	Turbo Heater Gas (psi)	Curtain Gas (psi)
Ceratamine A	40	10	20
	40	10	20
Ceratamine B	40	10	30
	40	10	30
Metoprolol	30	10	25
	30	10	25
Nicardipine	40	10	20
	40	10	20
Propranolol	40	10	30
	40	10	30
Verapamil	30	10	10
	30	10	10
Warfarin	30	10	10
	30	10	10

Table 2.3. MS-MS compound parameters used for the analysis of the ceratamines and the metabolic stability control compounds. Optimal conditions were determined by infusion.

Compound	$[M+H]^+$ (*m/z*)	Product Ion (*m/z*)	Declustering Potential (V)	Focusing Potential (V)
Ceratamine A	468.896	203.1	91	340
	468.896	161.9	91	340
Ceratamine B	454.852	189.0	26	370
	454.852	134.1	26	370
Metoprolol	268.168	116.0	21	370
	268.168	74.0	21	370
Nicardipine	480.036	315.0	21	360
	480.036	91.0	21	360
Propranolol	260.1	116.2	21	370
	260.1	183.2	21	370
Verapamil	455.238	165.0	36	370
	455.238	150.1	36	370
Warfarin	309.059	163.2	26	370
	309.059	250.9	26	370

Table 2.4. Additional MS-MS compound parameters used for the analysis of the ceratamines and the metabolic stability control compounds. Optimal conditions were determined by infusion.

Compound	Collision Energy (arbitrary units)	Collision Cell Exit Potential (V)	Entrance Potential (V)
Ceratamine A	37	8	4
	45	6	4
Ceratamine B	37	6	5.5
	67	2	5.5
Metoprolol	25	4	4.5
	37	8	4.5
Nicardipine	29	16	12
	79	10	12
Propranolol	25	4	4.5
	27	6	4.5
Verapamil	33	8	7.5
	49	6	7.5
Warfarin	19	6	6.5
	23	6	6.5

A multiple reaction monitoring method was developed for ceratamine A. This method involved monitoring the following seven transitions: 441→175, 441→189, 455→189, 455→203, 469→203, 471→189, and 483→203.

2.3.2.2 LC-quadrupole-time-of-flight (QqTOF) analysis

A Shimadzu Prominence LC equipped with a UV detector and coupled to a QSTAR Elite QqTOF mass spectrometer with a turboion spray source (Applied Biosystems/MDS Sciex, Foster City, CA) was used to identify all metabolites and obtain accurate mass data. Separations were accomplished using a ThermoFisher C18 column (150 x 2.1 mm, 5 µM particle diameter). Mobile phase A was H_2O containing 0.1% acetic acid. Mobile phase B was CH_3CN. A total flow rate of 0.2 mL/min was used. Typical injection volumes were 25 µL, however 40 µL injections were performed for accurate mass determinations of very minor metabolites. UV analysis was performed using a wavelength of 350 nm.

The mobile phase gradient used for the separation of ceratamine A metabolites was as follows: 3 min hold at 15% CH_3CN, increase to 17% CH_3CN over 1 min, 18 min hold at 17% CH_3CN, increase to 27% CH_3CN over 1 min, 4 min hold at 27% CH_3CN, increase to 35% CH_3CN over 2 min, 11 min hold at 35% CH_3CN, decrease to 15% CH_3CN over 2 min, 3 min hold at 15% CH_3CN.

The mobile phase gradient used for the separation of ceratamine B metabolites was as follows: 3 min hold at 15% CH_3CN, increase to 25% CH_3CN over 1 min, 5 min hold at 25% CH_3CN, increase to 35% CH_3CN over 1 min, 11 min hold at 35% CH_3CN, decrease to 15% CH_3CN over 1 min, 3 min hold at 15% CH_3CN.

Ideal MS parameters were determined by infusion of each compound. For metabolites of ceratamine A: IonSpray voltage was 5300 V, source temperature was 450 °C, declustering potential was 70 V, and focusing potential was 225 V. A collision energy of 30 (arbitrary units) was used for CA-M3. A collision energy of 35 (arbitrary units) was used for all other metabolites of ceratamine A.

For metabolites of ceratamine B: IonSpray voltage was 5300 V, source temperature was 425 °C, declustering potential was 70 V, and focusing potential was 300 V. A collision energy of 35 (arbitrary units) was used for all metabolites of ceratamine B.

Accurate mass determinations were performed using a QSTAR Elite QqTOF mass spectrometer. The monoisotopic $[M+H]^+$ ion signal from the corresponding parent compound was used as an accurate mass calibrant (ceratamine A: 466.9713 Da; ceratamine B: 452.9556 Da).

2.3.3 UV/Vis analysis

UV/Vis spectra were collected using a Perkin Elmer Lambda 35 dual beam UV/Vis spectrometer. Absorbance values were measured over a range of 200-700 nm. A slit width of 1 nm and a scan speed of 480 nm/min was utilized. Water was used as the background reference.

2.3.4 ^{1}H NMR analysis

^{1}H NMR spectra were collected using a Brüker 600 MHz NMR equipped with a 5 mm cryoprobe. DMSO-d_6 was used as a solvent for all NMR analysis.

3.0 STRUCTURE ELUCIDATION OF PHASE I METABOLITES OF THE MICROTUBULE PERTURBAGENS: CERATAMINES A AND B

3.1 PHASE I METABOLISM OF CERATAMINES A AND B IN RAT LIVER MICROSOMES

To date there have been no reported studies on the pharmacokinetics of the ceratamines, therefore the initial goal was to perform a qualitative study focused on identifying phase I metabolites of each compound.[43] Rat liver microsomes were chosen as they are a rich source of cytochromes P450, a large family of enzymes that are heavily involved in drug metabolism.[37] Metabolites of the ceratamines were found to be formed within 15 min of addition of the co-factor NADPH. Several control incubations were performed using heat inactivated and boiled microsomes to ensure the chemical stability of each compound. Species that were only detected within an active enzyme system in the presence of NADPH and not in the chemical stability controls were considered for structure elucidation.

Reversed phase HPLC was used to separate the newly formed metabolites, with UV being the initial detection method. The chromatograms suggested the presence of at least seven metabolites of ceratamine A and five metabolites of ceratamine B after 60 min of incubation with rat liver microsomes (Figure 3.1).

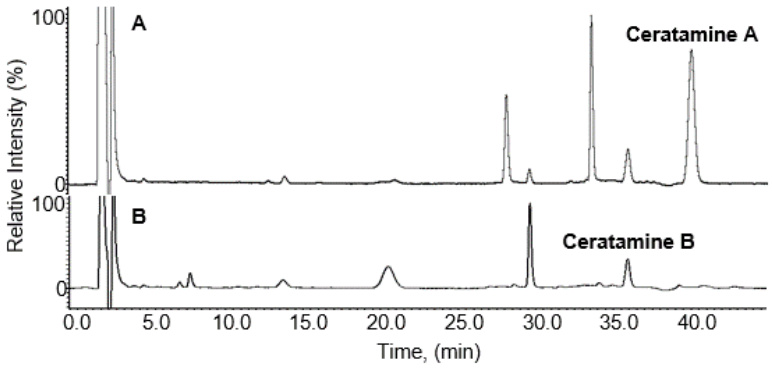

Figure 3.1. RP HPLC-UV chromatograms of 60 min rat microsomal incubations of (A) ceratamine A and (B) ceratamine B [Adapted with permission from Smith *et* al., *Journal of Natural Products*, **2014**, *77*, 1572-1578.[43] Copyright (2014) American Chemical Society.].

3.2 PRELIMINARY STRUCTURE ELUCIDATION OF PHASE I METABOLITES OF CERATAMINES A AND B

Initial structure elucidation was performed using tandem mass spectrometry.[43] Although the structures of the metabolites were unknown, the types of metabolic reactions were limited to phase I due to the enzyme source and cofactor. Phase I metabolism typically involves simple reactions, leaving the majority of the compound unchanged.[37] Therefore, potential metabolites should share similar MS characteristics with the parent drugs.

3.2.1 MS spectra of ceratamines A and B

The molecular ion, $[M+H]^+$, of each of the ceratamines appeared as three ion signals with a 1:3:1 intensity ratio (Figure 3.2). This ratio corresponds with the presence of two bromine atoms and also served as a useful marker for metabolite identification. Each compound was fragmented into

several product ions via collision induced dissociation (CID). The major CID product ions of interest were *m/z* 203 and 189 for ceratamine A and B, respectively.

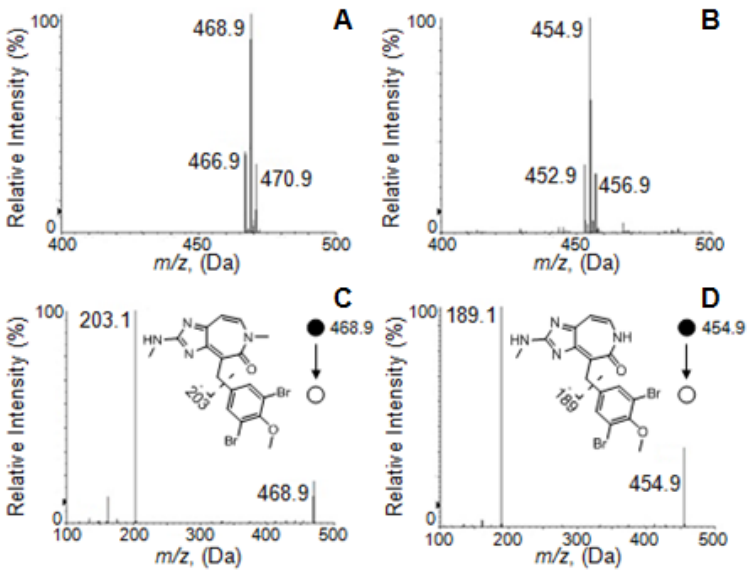

Figure 3.2. $[M+H]^+$ ion clusters of (A) ceratamine A and (B) ceratamine B; CID product ions of (C) ceratamine A and (D) ceratamine B [Adapted with permission from Smith *et* al., *Journal of Natural Products*, **2014**, *77*, 1572-1578.[43] Copyright (2014) American Chemical Society.].

These ions were the result of a neutral loss of 264, indicating dissociation at the benzylic position (Figure 3.3). This was also supported by accurate mass determinations and fragmentation prediction via PeakView® software from ABSciex (Appendix A Table A1).

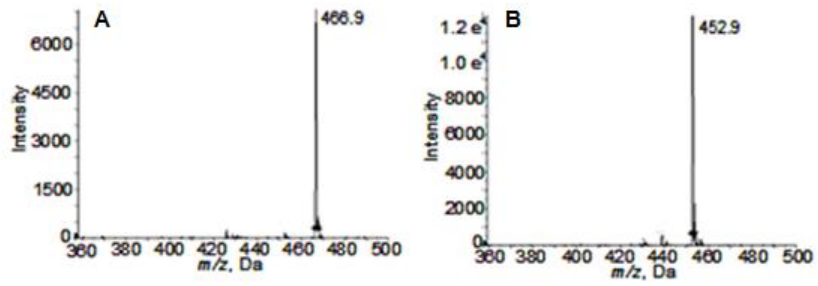

Figure 3.3. Neutral loss scans confirming the fragmentation of the ceratamines resulted in a loss of 263.88 Da; (A) ceratamine A, (B) ceratamine B [Adapted with permission from Smith *et* al., *Journal of Natural Products*, **2014**, *77*, 1572-1578.[43] Copyright (2014) American Chemical Society.].

The presence of three ion signals with a 1:3:1 isotopic intensity ratio was used as a marker for metabolites of the ceratamines. The difference in the *m/z* values of the molecular ions was then utilized to determine the type of structural change. The location of the structural change(s) was determined by comparing the major product ions of each metabolite to the parent compound.

3.2.2 Metabolites of ceratamine B

Quadrupole-time-of-flight (QqTOF) mass spectrometry was used as the second method of detection to identify metabolites. QqTOF instruments offer an increased sensitivity in full scan mode due to an improved duty cycle. QqTOF-MS was used to identify the precursor and major product ion of each metabolite. Five phase I metabolites were identified using both UV and QqTOF-MS detection, having molecular ion differences of +2, −28, +16, and −14 Da from the parent compound, ceratamine B. (Table 3.1).

Table 3.1. Chromatographic and mass spectrometric information of metabolites of ceratamine B used for structure elucidation [Adapted with permission from Smith *et* al., *Journal of Natural Products*, **2014**, *77*, 1572-1578.[43] Copyright (2014) American Chemical Society.].

Analyte	t_r (min)	$[M+H]^+$ (*m/z*)	Mass Difference from ceratamine B $[M+H]^+$ (*m/z*)	Major CID product ion (*m/z*)
M1	6.3	455, 457, 459	+2	175
M2	7.2	425, 427, 429	−28	175
M3	9.4	469, 471, 473	+16	189
M4	10.9	439, 441, 443	−14	189
M6	14.1	439, 441, 443	−14	189
Ceratamine B	18.9	453, 455, 457	--	189

Metabolite 1 (M1). Metabolite 1 had a monoisotopic *m/z* of 455, which is a +2 Da difference from ceratamine B (Figure 3.4). This molecular weight difference was noticed in the analysis of ceratamine A and was determined to be consistent with a demethylation and monooxygenation. The major CID product ion of *m/z* 175, indicated that the demethylation occurred within the imidazoazepinone (Figure 3.4). The only likely site of dealkylation is at the aminoimidazole. Fragmentation supports that the monooxygenation occurred on the aromatic ring, however the specific site and type of reaction cannot be determined using tandem mass spectrometry.

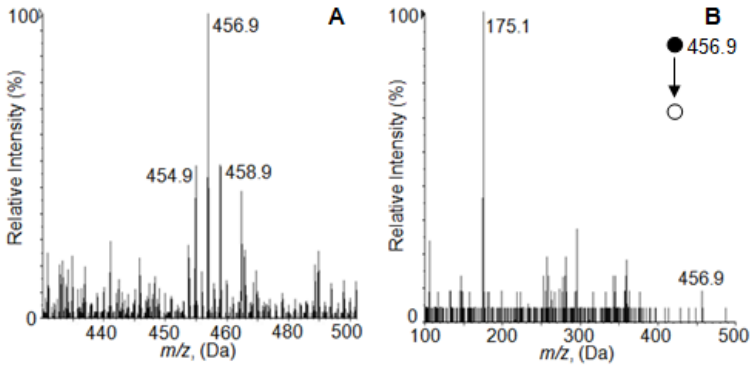

Figure 3.4. (A) $[M+H]^+$ ion cluster of M1, (B) CID product ions of M1 [Adapted with permission from Smith *et* al., *Journal of Natural Products*, **2014**, *77*, 1572-1578.[43] Copyright (2014) American Chemical Society.].

Metabolite 2 (M2). Metabolite 2 had a −28 Da molecular ion difference when compared with ceratamine B. The monoisotopic *m/z* was 425, which is consistent with a double demethylation (Figure 3.5). The major CID product ion had an *m/z* value of 175, indicating that one demethylation occurred within the imidazoazepinone (Figure 3.5). M2 was determined to be the result of a demethylation at the aminoimidazole and the methoxy.

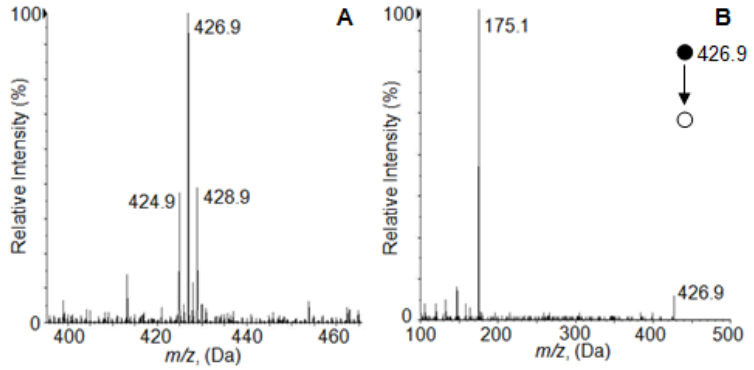

Figure 3.5. (A) $[M+H]^+$ ion cluster of M2, (B) CID product ions of M2 [Adapted with permission from Smith *et* al., *Journal of Natural Products*, **2014**, *77*, 1572-1578.[43] Copyright (2014) American Chemical Society.].

Metabolite 3 (M3). The third phase I metabolite of ceratamine B had a monoisotopic *m/z* of 469, which is a difference of +16 Da from the parent (Figure 3.6). This is consistent with a monooxygenation. The major CID product ion of *m/z* 189 suggested that this structural change occurred on the aromatic ring, although the site and type of reaction could not be determined (Figure 3.6).

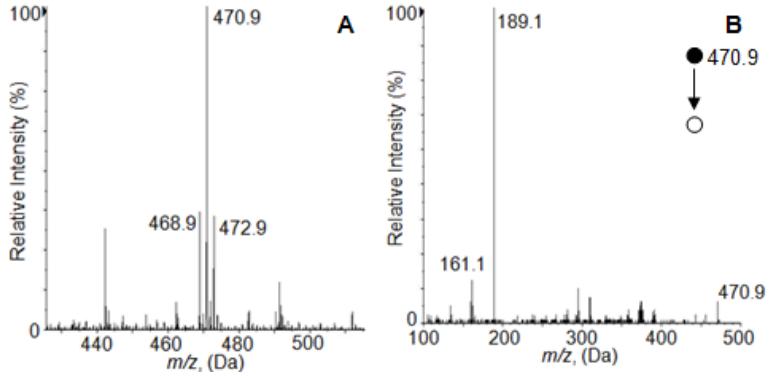

Figure 3.6. (A) $[M+H]^+$ ion cluster of M3, (B) CID product ions of M3 [Adapted with permission from Smith *et* al., *Journal of Natural Products*, **2014**, *77*, 1572-1578.[43] Copyright (2014) American Chemical Society.].

Metabolites 4 and 6 (M4 and M6). The major metabolites of ceratamine B were isobaric species with monoisotopic *m/z* values of 439 (Figure 3.7). They share a difference of −14 Da from ceratamine B itself. This is consistent with a demethylation, which could occur at the aminoimidazole or the methoxy. To determine this location, the major product ions were compared with the parent. M4 fragmented to the same major CID product ion as ceratamine B, *m/z* 189. This allowed for the conclusion that M4 was formed through demethylation at the methoxy. M6 had a major CID product ion of *m/z* 175, which is a loss of 14 Da from that of ceratamine B. M6 was determined to be the result of demethylation at the aminoimidazole.

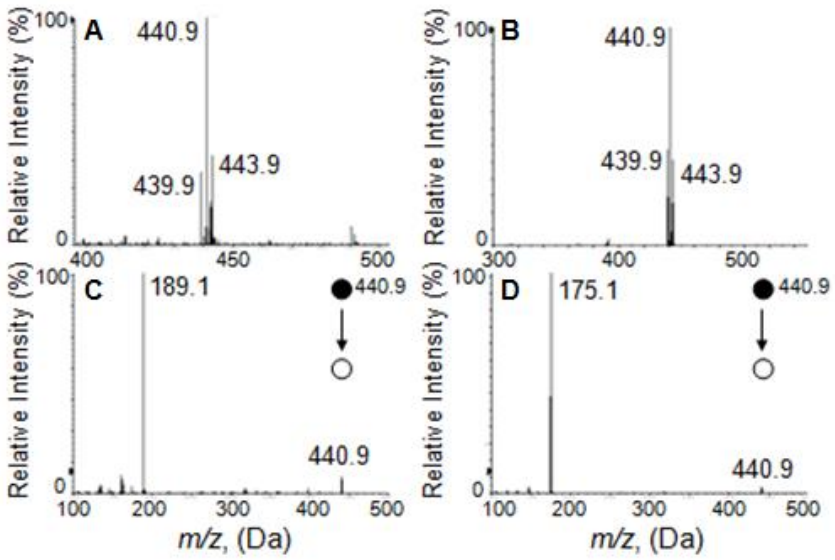

Figure 3.7. $[M+H]^+$ ion clusters of (A) M4 and (B) M6; CID product ions of (C) M4 and (D) M6 [Adapted with permission from Smith *et* al., *Journal of Natural Products*, **2014**, *77*, 1572-1578.[43] Copyright (2014) American Chemical Society.].

3.2.3 Metabolites of ceratamine A

The only structural difference between the ceratamines is the presence of a methyl group at the amide position. Since ceratamine A has an additional site for demethylation, it is expected to have a similar, yet more complex metabolic profile. Although a total of eight phase I metabolites were initially detected, there were only four differences in the *m/z* values of molecular ions (Table 3.2). Therefore, many isobaric species were present which led to challenges in structure elucidation.

Table 3.2. Chromatographic and mass spectrometric information of metabolites of ceratamine A used for structure elucidation [Adapted with permission from Smith *et* al., *Journal of Natural Products*, **2014**, *77*, 1572-1578.[43] Copyright (2014) American Chemical Society.].

Analyte	t_r (min)	$[M+H]^+$ (*m/z*)	Mass Difference from ceratamine A $[M+H]^+$ (*m/z*)	Major CID product ion (*m/z*)
M4	22.1	439, 441, 443	−28	189
M5	28.4	453, 455, 457	−14	203
M6	29.3	439, 441, 443	−28	175
M7	33.3	453, 455, 457	−14	189
CB	36.3	453, 455, 457	−14	189
M8	20.8	483, 485, 487	+16	203
M9	11.5	469, 471, 473	+2	189
M10	12.8	439, 441, 443	−28	189
Ceratamine A	41.1	467, 469, 472	--	203

When examining the structure of ceratamine A, there are several sites that would be expected to be metabolically labile. Dealkylation reactions are more likely to occur adjacent to a heteroatom; therefore the secondary amine, tertiary amide, and methoxy groups of ceratamine A are all expected to be sites of demethylation.[37] Ceratamine A also contains an aromatic ring, which is a probable site for hydroxylation.[37]

Metabolite 9 (M9). M9, a metabolite unique to ceratamine A, had the shortest retention time, indicating it to be the most polar metabolite. The molecular ions differed from the parent by +2 Da and had *m/z* values of 469, 471, and 473 (Figure 3.8). This metabolite was most likely formed through two metabolic reactions; monooxygenation and demethylation.

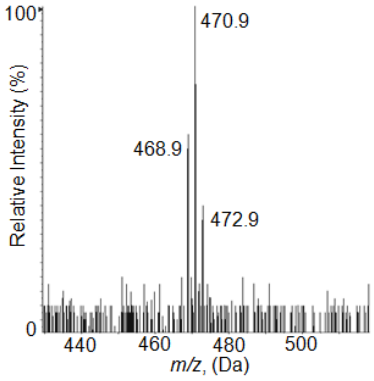

Figure 3.8. $[M+H]^+$ ion cluster of M9.

The major CID product ion of M9 was *m/z* 189, which differed by −14 Da from the major product ion of ceratamine A (Figure 3.8). This difference suggests that the demethylation occurred on the imidazoazepinone; therefore, demethylation of the methoxy group can be excluded. Unfortunately, during this initial analysis the specific site of demethylation could not be confirmed; however, this was eventually determined after the development of a multiple reaction monitoring (MRM) method discussed later.

The major product ion also suggested that the monooxygenation occurred on the aromatic portion of the molecule; however, the type of monooxygenation and specific site cannot be determined by tandem mass spectrometry.

Metabolites 10, 4, and 6 (M10, M4, M6). The molecular ions of these three isobaric metabolites differed from the parent by a loss of 28 Da. (Figure 3.9). These metabolites are consistent with the loss of two methyl groups.

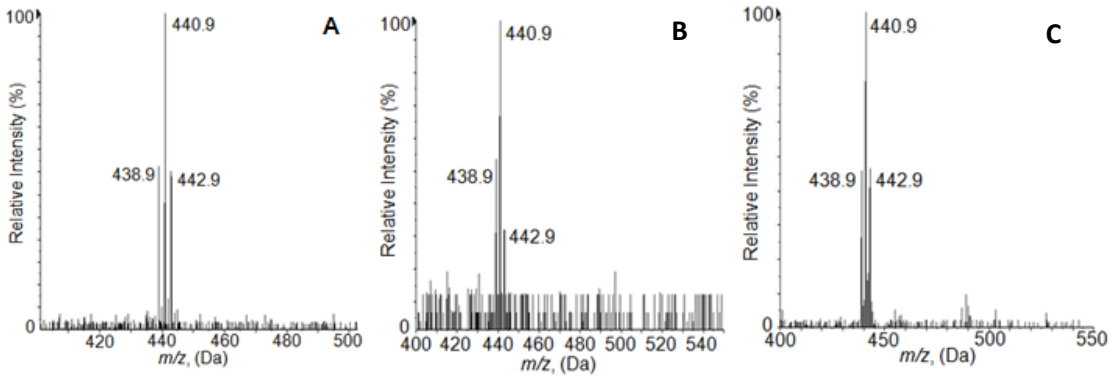

Figure 3.9. $[M+H]^+$ ion clusters of (A) M10, (B) M4, and (C) M6. [Adapted with permission from Smith *et* al., *Journal of Natural Products*, **2014**, *77*, 1572-1578.[43] Copyright (2014) American Chemical Society.]

The major CID product ion of M10 and M4 was *m/z* 189, a −14 Da difference from the major product ion of ceratamine A (Figure 3.10). This indicates that only one demethylation reaction occurred within the imidazoazepinone. The second demethylation reaction must have occurred at the methoxy group, which would not result in a mass change of the product ion.

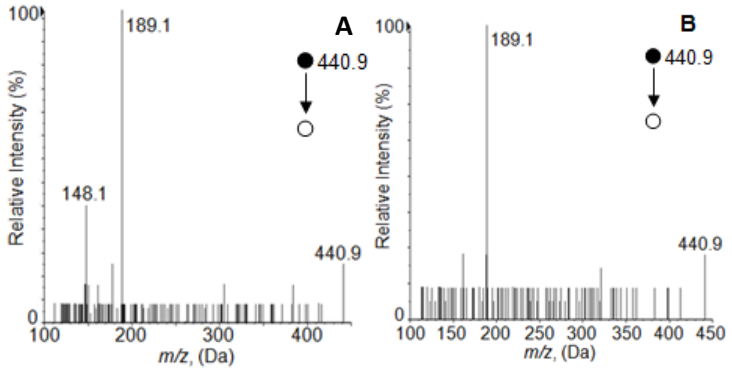

Figure 3.10. CID product ions of (A) M10, and (B) M4.

Understanding the effect of various demethylations of the ceratamines on the relative polarity of the molecule was important to differentiate between isobaric metabolites, specifically those with a demethylation at the aminoimidazole or at the tertiary amide. A simple experiment

was performed that involved analyzing ceratamine B with the same chromatographic conditions used to separate ceratamine A metabolites. This experiment revealed that a demethylation at the aminoimidazole would result in a larger increase in polarity, therefore the elution order of isobaric species can be used to differentiate between these sites of demethylation (Figure 3.11).

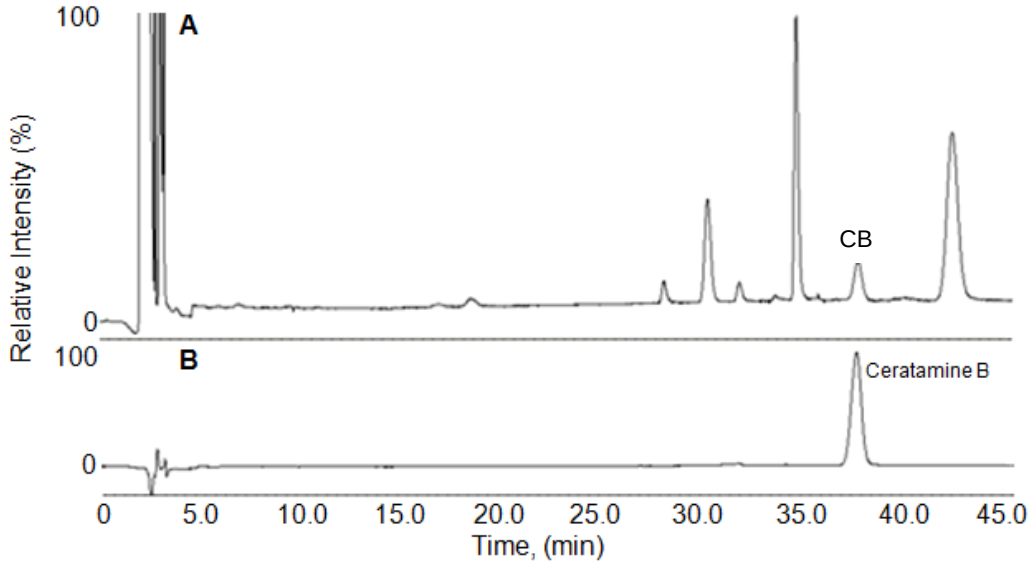

Figure 3.11. Comparison of retention times of ceratamine B to CB. (A) 60 min incubation of ceratamine B with rat liver microsomes, (B) 10 µM standard of ceratamine B. This experiment revealed that a demethylation at the aminoimidazole resulted in a shorter retention time and therefore a larger increase in polarity [Adapted with permission from Smith *et* al., *Journal of Natural Products*, **2014**, *77*, 1572-1578.[43] Copyright (2014) American Chemical Society.].

M10 was the most polar of the three double demethylated metabolites, therefore it was determined to be the result of demethylation at the aminoimidazole and the methoxy. M4 resulted from a demethylation at the tertiary amide and the methoxy. Finally, M6 had a major CID product ion of *m/z* 175, which is consistent with demethylation at the aminoimidazole and tertiary amide.

Metabolite 8 (M8). Metabolite 8 was a very minor metabolite that had a monoisotopic *m/z* of 483, a gain of 16 Da when compared to the parent. (Figure 3.12) This is most likely the result of monooxygenation. The major CID product ion of M8 was equivalent to that of ceratamine A; *m/z* of 203 (Figure 3.12). Therefore, the structural change occurred on the aromatic ring, however the type of reaction and specific site cannot be determined by tandem mass spectrometry.

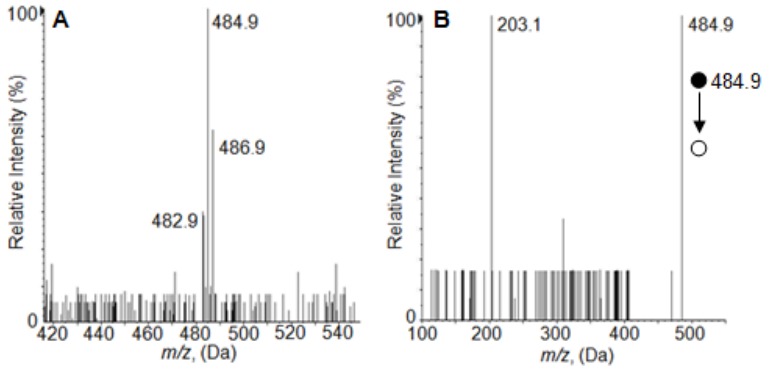

Figure 3.12. (A) $[M+H]^+$ ion cluster of M8, (B) CID product ions of M8 [Adapted with permission from Smith *et* al., *Journal of Natural Products*, **2014**, *77*, 1572-1578.[43] Copyright (2014) American Chemical Society.].

Metabolites 5, 7 and CB (M5, M7, CB). The final three phase I metabolites of ceratamine A, formed by rat liver microsomes, were isobaric with a monoisotopic *m/z* value of 453 (Figure 3.13). This difference of −14 Da is indicative of a demethylation reaction.

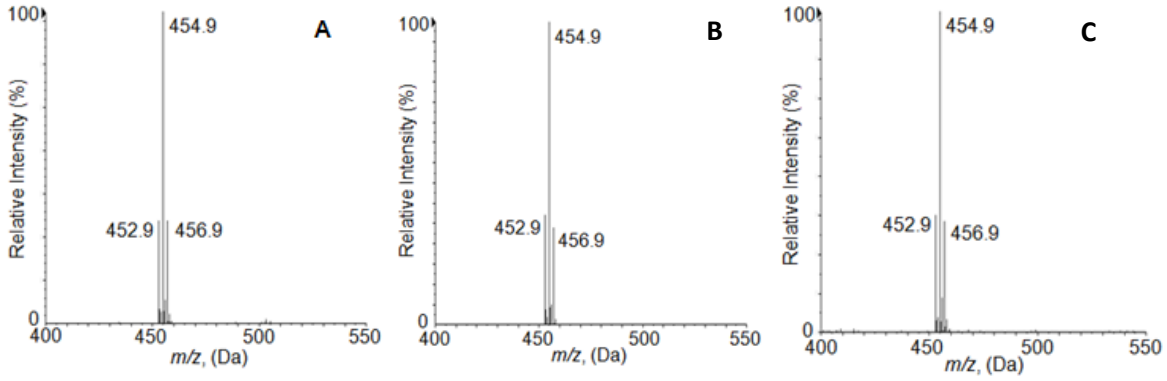

Figure 3.13. $[M+H]^+$ ion clusters of (A) M5, (B) M7, and (C) CB [Adapted with permission from Smith *et* al., *Journal of Natural Products*, **2014**, *77*, 1572-1578.[43] Copyright (2014) American Chemical Society.].

The major product ions were essential in determining the location of dealkylation. M5 fragmented to form *m/z* 203, which is the same product ion as ceratamine A (Figure 3.14). Therefore, M5 is the result of a demethylation at the methoxy. M7 and CB shared the same major CID product ion of *m/z* 189, a loss of 14 Da from the major CID product ion of ceratamine A (Figure 3.14). Due to the correlation between polarity and retention time, it was concluded that M7 was the result of demethylation at the aminoimidazole and CB was the result of demethylation at the tertiary amide.

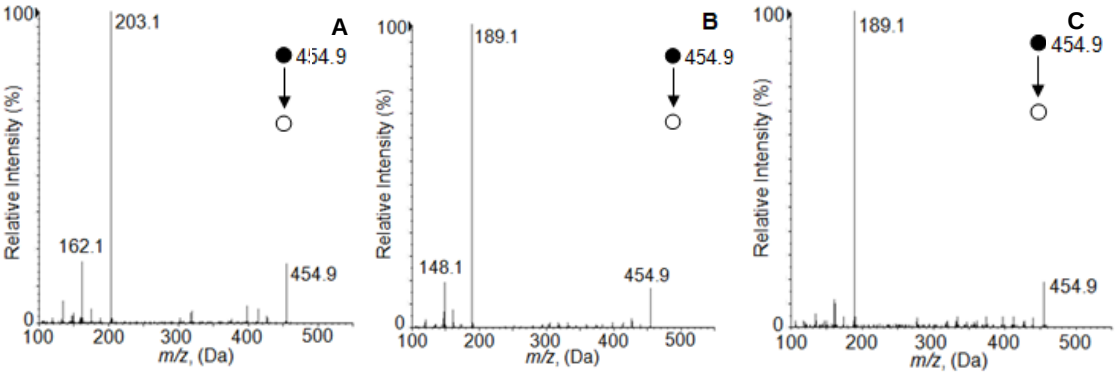

Figure 3.14. CID product ions of (A) M5, (B) M7, and (C) CB [Adapted with permission from Smith *et* al., *Journal of Natural Products*, **2014**, *77*, 1572-1578.[43] Copyright (2014) American Chemical Society.].

3.2.4 Multiple reaction monitoring (MRM) of metabolites of the ceratamines

As previously mentioned, structure elucidation was achieved by comparing molecular ions and major product ions of each metabolite to the parent compounds. This analysis was performed using a QqTOF-MS, which allows for a highly sensitive full scan due to an improved duty cycle. After this information was obtained, a MRM method was developed for each compound and their corresponding metabolites using a triple quadrupole tandem mass spectrometer.

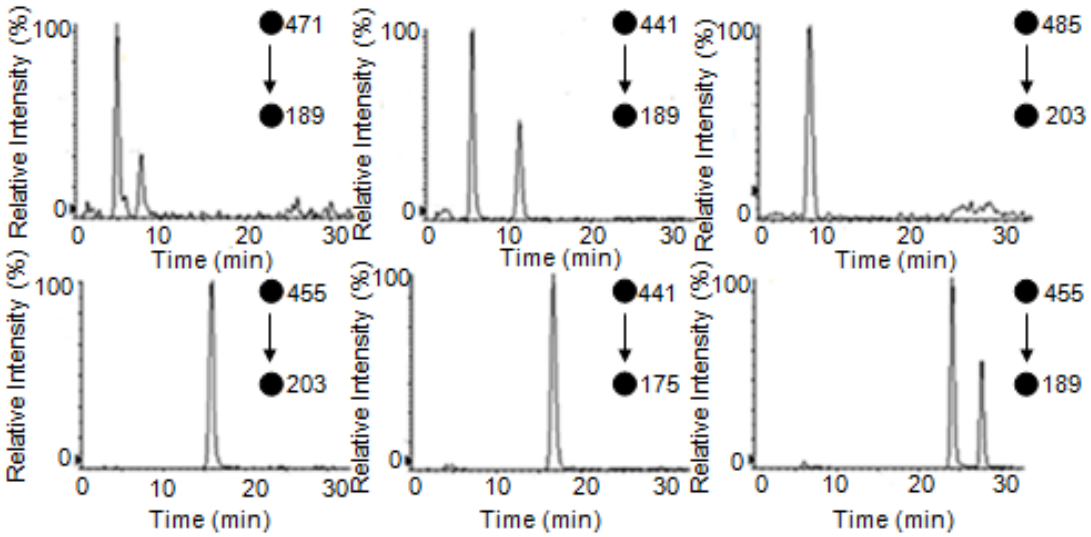

Figure 3.15. MRM analysis of metabolites of Ceratamine A formed by rat liver microsomes. Incubation time: 90 min.

An additional, very minor metabolite was identified for ceratamine A that was not detected during initial analysis (Figure 3.15). M11 had a MRM transition identical with that of M9 (471 → 189). The identification of this metabolite allowed the structure of both M9 and M11 to be deduced. Due to its slightly longer retention time, M11 is most likely the result of a demethylation at the tertiary amide and monooxygenation along the aromatic ring; therefore, M9

is most likely the result of a demethylation at the aminoimidazole and monooxygenation along the aromatic ring. No additional metabolites were detected for Ceratamine B using the MRM method (Figure 3.16).

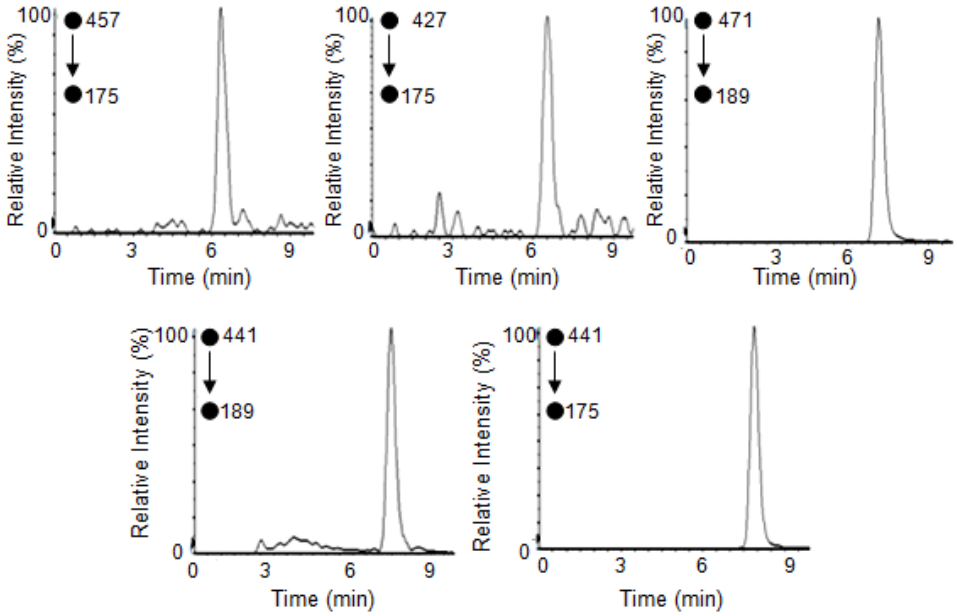

Figure 3.16. MRM analysis of metabolites of Ceratamine B formed by rat liver microsomes. Incubation time: 60 min.

The ceratamines were both significantly metabolized by rat liver microsomes. Ceratamine A was found to be converted to nine phase I metabolites, while five phase I metabolites were formed for ceratamine A. Preliminary structure elucidation via tandem mass spectrometry was successful in determining the structures of various demethylated metabolites, however it was not sufficient in identifying the specific structure of any monooxygenated metabolites. Figure 3.17 displays the proposed structures of the phase I metabolites of the ceratamines.

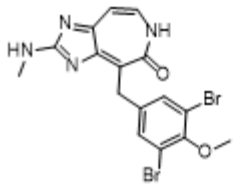

Ceratamine A

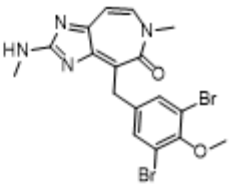

Ceratamine B

Major Metabolites

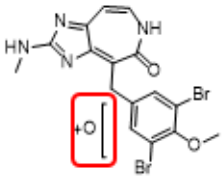

M3

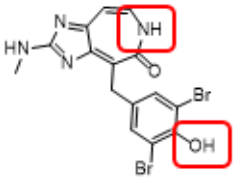

M4

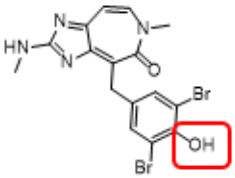

M5

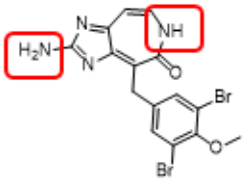

M6

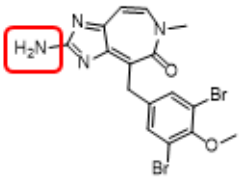

M7

Minor Metabolites

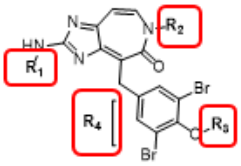

M1: R_1: H; R_2: H; R_3: CH_3; R_4: +O
M2: R_1: H; R_2: H; R_3: H; R_4: ---
M8: R_1: CH_3; R_2: CH_3; R_3: CH_3; R_4: +O
M9: R_1: H; R_2: CH_3; R_3: CH_3; R_4: +O
M10: R_1: H; R_2: CH_3; R_3: H; R_4: ---
M11: R_1: CH_3; R_2: H; R_3: CH_3; R_4: +O
CB: R_1: CH_3; R_2: H; R_3: CH_3; R_4: ---

Figure 3.17. Proposed structures of the phase I metabolites of the ceratamines.

3.3 CONFIRMATORY STRUCTURE ELUCIDATION OF PHASE I METABOLITES OF CERATAMINES A AND B

Although many metabolites were identified in the preliminary studies, the focus of confirmatory structure elucidation methods was on the major metabolites of each of the ceratamines and also on any metabolites that were found to be formed by both compounds.

3.3.1 Co-injection experiment

In order to identify any similarities in the metabolites formed by each compound, a co-injection experiment was performed (Figure 3.18). The co-injection experiment resulted in the identification of eight significant metabolites.

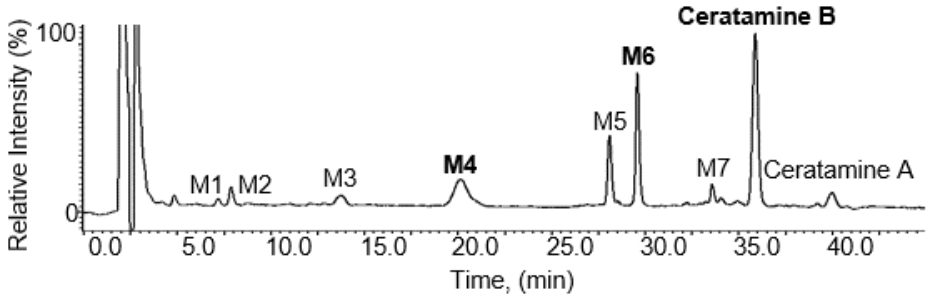

Figure 3.18. RP-HPLC-UV chromatogram of a co-injection of 60 min rat microsomal incubations of ceratamine A and B. The co-injection experiment suggests that two metabolites, M4 and M6, are formed for both compounds, and that a metabolite of ceratamine A, CB, has an identical retention time with ceratamine B [Adapted with permission from Smith *et* al., *Journal of Natural Products*, **2014**, *77*, 1572-1578.[43] Copyright (2014) American Chemical Society.].

M1-M3 were unique to ceratamine B, while M4 and M6 were common to both compounds. M5 and M7 were unique to ceratamine A. An additional metabolite of ceratamine A, labeled as

CB, was found to have a retention time consistent with ceratamine B. Since the biological activity of ceratamine B has already been established, this observation suggests the possibility of ceratamine A to behave as a pro-drug.

The metabolites of interest for confirmatory structure elucidation were selected based on relative abundance, which was calculated by comparing the peak area of the metabolite to the peak area of the parent drug (Table 3.3).

Table 3.3. Relative abundances of phase I metabolites of the ceratamines after 60 min incubations with rat liver microsomes [Adapted with permission from Smith *et* al., *Journal of Natural Products*, **2014**, *77*, 1572-1578.[43] Copyright (2014) American Chemical Society.].

Analyte	**Relative Abundance (%)**	
	Ceratamine A	Ceratamine B
M1	----	0.9
M2	----	3.2
M3	----	3.3
M4	0.4	15.6
M5	12.4	----
M6	1.9	23.6
M7	24.3	----
CB	5.8	----

3.3.2 Accurate mass determinations

Accurate mass determinations were performed using TOF-MS in order to support the proposed molecular formulas of the metabolites of the ceratamines (Table 3.4). The parent compounds were used as internal accurate mass calibrants (Ceratamine A + H, 466.97127 Da; Ceratamine B + H: 452.95562 Da). With errors typically below 5 ppm, the proposed molecular formulas were supported by accurate mass.

Table 3.4. Accurate mass determination results for proposed molecular formulas of metabolites of the ceratamines [Adapted with permission from Smith *et* al., *Journal of Natural Products*, **2014**, *77*, 1572-1578.[43] Copyright (2014) American Chemical Society.].

Analyte	Proposed Molecular Formula	Experimentally determined monoisotopic ion signal (*m/z*)	Theoretical monoisotopic mass (Da)	Error (ppm)
M1	$C_{15}H_{12}Br_2N_4O_3$	454.9357	454.9349	1.8
M2	$C_{15}H_{12}Br_2N_4O_3$	424.9235	434.9243	1.9
M3	$C_{16}H_{14}Br_2N_4O_3$	468.9486	468.9505	4.1
M4	$C_{15}H_{12}Br_2N_4O_2$	438.9395	438.9400	1.1
M5	$C_{16}H_{14}Br_2N_4O_2$	452.9570	452.9556	3.1
M6	$C_{15}H_{12}Br_2N_4O_2$	438.9391	438.9400	2.0
M7	$C_{16}H_{14}Br_2N_4O_2$	452.9533	452.9556	5.1
CB*	$C_{16}H_{14}Br_2N_4O_2$	452.9577	452.9556	4.6

*Source of ceratamine B was from an incubation of ceratamine A with rat liver microsomes.

3.3.3 Isolation of major metabolites of ceratamine B

In order to additionally support the proposed structures of the major metabolites of ceratamine B formed by rat liver microsomes, a proper isolation method needed to be developed. Due to the somewhat polar nature of the ceratamines, reversed phase HPLC was found to be an effective method of separation. Therefore, semi-preparative HPLC was chosen for the isolation of metabolites. Incubation conditions were also modified in order to increase the relative abundances of each metabolite. Optimal conditions for the large scale incubations were determined to be a drug concentration of 50 µM, a five-fold increase from the traditional method. Microsomal protein concentration was increased to 2 mg/mL (0.094 nmol P450/mg protein). A final concentration of 1 mM NADPH was still utilized, however cofactor was added after every 15 min to ensure an excess throughout the reaction. A 60 min incubation was performed with a total volume of 5 mL. Figure 3.19 displays a chromatogram obtained using the optimized mobile phase gradient for semi-preparative separation.

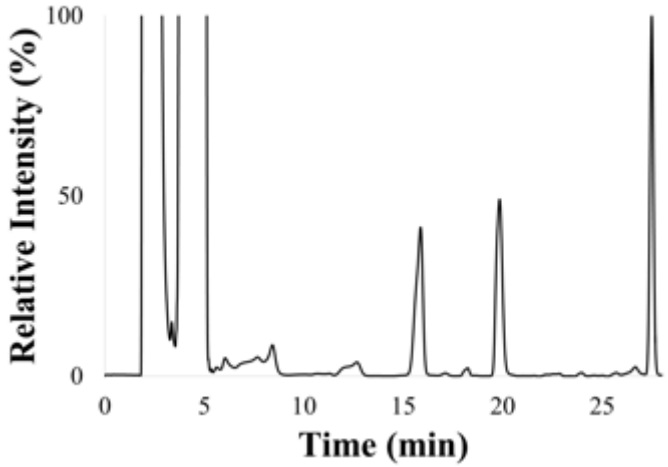

Figure 3.19. HPLC-UV chromatogram displaying optimized separation of metabolites of ceratamine B using a semi-preparative column. Incubation Conditions: [Drug]: 50 µM, [Rat liver microsomes]: 2 mg/mL (0.094 nmol P450/mg protein), [NADPH]: 1 mM (added every 15 min), 100 mM ammonium acetate buffer pH 7.4, incubated for 60 min at 37°C.

Semi-preparative separations require a significant increase in resolution as peak shape will be significantly affected by an increase in concentration and injection volume. In order to increase the efficiency of isolation, the effect of injection volume on peak shape and resolution was investigated. Figure 3.20 shows an overlay of chromatograms obtained using three different injection volumes: 50, 250, and 1000 µL.

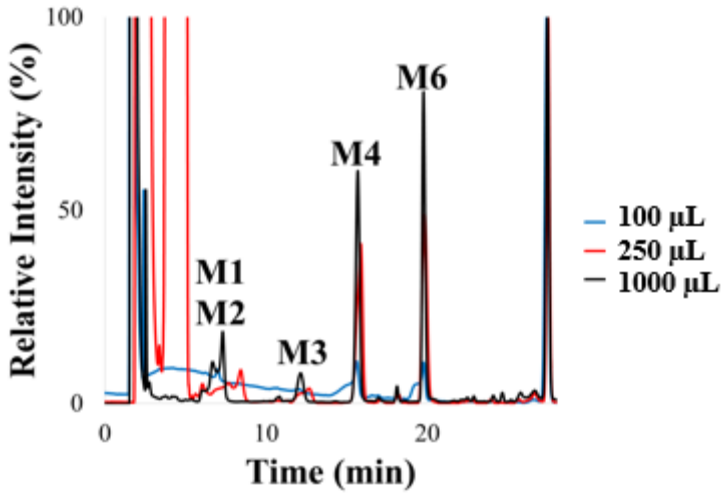

Figure 3.20. Effect of injection volume on separation of metabolites of ceratamine B using semi-preparative conditions.

3.3.4 UV/Vis spectroscopy

Absorbance data was collected for the three isolated metabolites of ceratamine B: M3, M4, and M6 (Figure 3.21). Two peaks observed within the UV range for all three metabolites and ceratamine B were considered to be the E and B bands, consistent with $\pi \rightarrow \pi^*$ transitions of the dibrominated benzene moiety. The high substitution of the benzene ring caused a bathochromic shift of the E band, allowing it to be observed within the UV region (λ_{max} ~203 nm). The B band of ceratamine B has a λ_{max} of 268 nm. The presence of an electron donating group, caused a red shift of the maximum absorbance of the B band.[44]

When comparing the E and B bands of the metabolites to ceratamine B, no major differences were noticed for M4 or M6. Preliminary structure elucidation suggested that M4 was formed as a result of a demethylation of the methoxy. Although this structural change occurred on the aromatic ring, M4 still contains an electron donating group, thus a significant change in

the B band was not expected.[42] M6 has been proposed to form as a result of a demethylation at the aminoimidazole. This would not result in any change to the aromatic ring, which is consistent with the observation of no significant shift in the absorbance of the B band.

Tandem mass spectrometry data supported the addition of an oxygen atom on the aromatic ring in order to form M3, however the exact structure of this monooxygenation could not be elucidated. When examining the absorbance data of M3, a hypsochromic shift was noticed at the B band. The addition of a hydroxy would be expected to increase delocalization and result in a bathochromic shift. Therefore, the observed hypsochromic shift does not support an aromatic hydroxylation. The loss of delocalization suggests that the metabolic reaction possibly resulted in a loss of aromaticity.

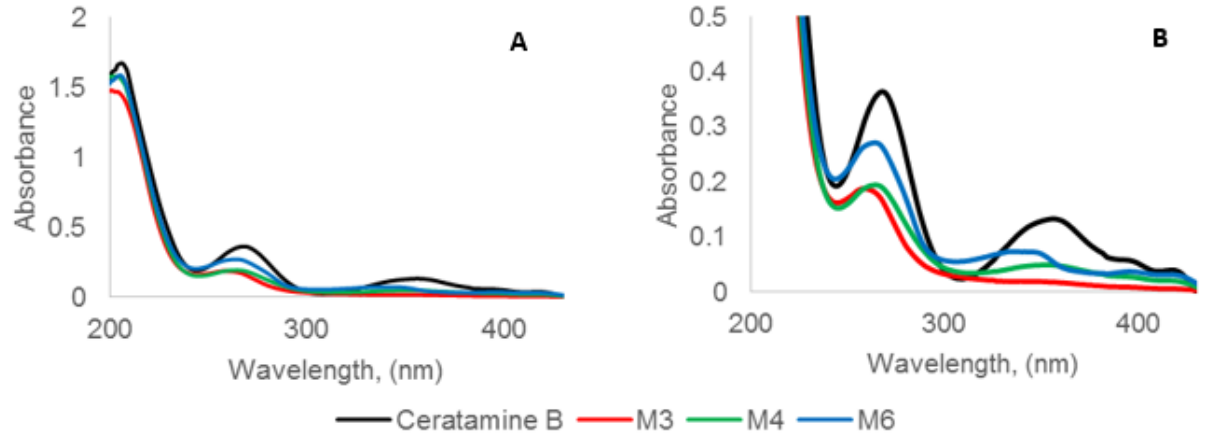

Figure 3.21. (A) UV-Vis absorbance spectra of ceratamine B, M3, M4 and M6 showing E band, B band, and imidazoazepinone band. (B) UV-Vis absorbance spectra of ceratamine B, M3, M4, and M6 focusing on the B band and imidazoazepinone band [Adapted with permission from Smith *et* al., *Journal of Natural Products*, **2014**, *77*, 1572-1578.[43] Copyright (2014) American Chemical Society.].

An additional absorbance band was noticed within the UV/Vis region for ceratamine B (λ_{max}: 357 nm). This band was attributed to a $\pi \rightarrow \pi^*$ transition of the highly conjugated imidazoazepinone portion of ceratamine B. No change was observed in this absorbance band for M3 or M4. Tandem mass spectrometry suggested no structural changes within the imidazoazepinone portion for either metabolite, therefore no shift in the visible band was expected. A hypsochromic shift (357 to 335 nm) was observed for M6, suggesting that a demethylation at the aminoimidazole, would result in a loss of delocalization.

3.3.5 ^{1}H NMR spectroscopy

^{1}H NMR was utilized to further confirm the proposed structures of the two major isolated metabolites, M4 and M6. Table 3.5 displays the ^{1}H NMR spectroscopic data for ceratamine B, M4, and M6. Ceratamine B contains a total of 15 protons at eight different positions (Figure 1.9; Appendix A, Figure A1). Preliminary structure elucidation suggested that M4 formed as a result of a demethylation at the methoxy. The ^{1}H NMR spectrum of M4 showed an absence of a singlet at δ 3.70, consistent with the loss of the methyl of the methoxy. The addition of a broad singlet at δ 6.57 was attributed to the resulting phenol (Appendix A, Figure A2).[44]

M6 was proposed to result from a demethylation of the aminoimidazole of ceratamine B. The ^{1}H NMR spectrum revealed an absence of a doublet at δ 3.07 ppm, consistent with the loss of the methyl at the aminoimidazole. Also, the multiplicity of the signal at δ 8.67 has changed from a broad quartet to a broad singlet (Appendix A, Figure A3). This change is due to the loss of any neighboring protons to the aminoimidazole, consistent with a demethylation.

Table 3.5. ^{1}H NMR Spectroscopic Data of ceratamine B, M4, and M6 [Adapted with permission from Smith *et* al., *Journal of Natural Products*, **2014**, *77*, 1572-1578.[43] Copyright (2014) American Chemical Society.].

Position	**Ceratamine B** δ_h, (*J* in Hz)	**M4** δ_h, (*J* in Hz)	**M6** δ_h, (*J* in Hz)
1	3.07, d (4.8)	3.06, d (5.4)	**n.d.**
2	8.67, q (broad) (4.8)	8.67, d (very broad)	**8.53, s (broad)**
3	6.42, d (9)	6.40, d (9)	6.48, d (9)
4	7.15, t (broad) (7.8)	7.10, d (broad) (9)	7.21, t (broad) (8.4)
5	11.40, d (broad) (6)	11.30, s (broad)	n.d.
6	4.17, s	4.10, s	4.15, s
7	7.70, s	7.90, s	7.95, s
8	3.70, s	**6.57, s**	3.73, s

n.d.: not detected

In conclusion, a total of eight metabolites were identified for the ceratamines. Preliminary structure elucidation, performed using tandem mass spectrometry, revealed that the majority of ceratamine metabolites are the result of various demethylation reactions. All proposed molecular formulas were supported by accurate mass. Monooxygenation was projected to occur in the formation of two metabolites, M1 and M3. MS-MS data suggested that the location of monooxygenation was along the aromatic ring. A hypsochromic shift in the B absorbance band of M3 revealed that the monooxygenation may result in a loss of aromaticity, however this observation needs to be further investigated before a structure can be proposed. Finally, the proposed structures of two major metabolites, M4 and M6, were confirmed by ^{1}H NMR (Figure 3.22).

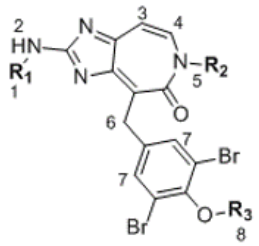

M4: R_1=CH_3, R_2=H, R_3=H
M6: R_1=H, R_2=H, R_3=CH_3
Ceratamine A: R_1=CH_3, R_2=CH_3, R_3=CH_3
Ceratamine B: R_1=CH_3, R_2=H, R_3=CH_3

Figure 3.22. Proposed structures of two major phase I metabolites of ceratamine B formed by rat liver microsomes. Structure elucidation was accomplished via tandem mass spectrometry, UV/Vis and ^{1}H NMR spectroscopy [Adapted with permission from Smith *et* al., *Journal of Natural Products*, **2014**, *77*, 1572-1578.[43] Copyright (2014) American Chemical Society.].

4.0 SPECIES COMPARISON OF METABOLIC PROFILE AND STABILITY OF THE MICROTUBULE PERTURBAGENS: CERATAMINES A AND B

An important part of the pre-clinical development of new chemical entities is the understanding of metabolite formation. Preliminary studies typically begin in species such as rat or mouse, as these are often utilized for initial *in vivo* studies.[37] However, since the overall goal of the discovery process is the approval of new drugs for use in humans, it is important to consider any species differences in metabolism. Performing *in vitro* metabolism studies with systems such as human liver microsomes early in pre-clinical development can be effective in revealing potential problems that may not have been noticed until clinical trials. At this earlier stage it is much easier and more cost effective to optimize lead compounds to avoid problems such as metabolic activation or stability.

4.1 SEMI-QUANTITATIVE EVALUATION OF THE METABOLISM OF THE CERATAMINES IN RAT LIVER MICROSOMES

The ceratamines were both found to be significantly metabolized by rat liver microsomes, with nine metabolites identified for ceratamine A and five for ceratamine B. The metabolism of each compound was monitored over 60 min in order to further understand the formation of each metabolite (Figure 4.1).

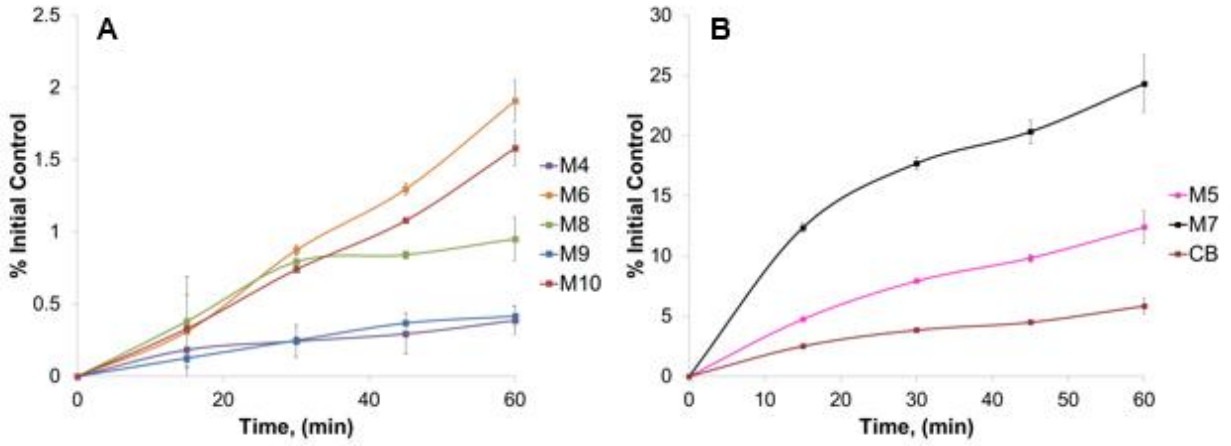

Figure 4.1. Formation of metabolites of ceratamine A by rat liver microsomes (0.01 nmol P450/mg protein). (A) minor metabolites, (B) major metabolites.

Due to the lack of pure standards of each metabolite for optimization of MS source and compound conditions, the analysis of these semi-quantitative assays was accomplished using the UV trace, as it is more likely that the phase I metabolites of the ceratamines would have similar UV absorbance than similar ionization characteristics.

Figure 4.1 displays the formation of eight of the nine phase I metabolites of ceratamine A formed by rat liver microsomes. M11 will not be further discussed as it is a very minor metabolite that is below the limit of detection of the UV analysis method. The major metabolites of ceratamine A were found to be M5, M7, and CB. All three of these metabolites were formed as the result of a single metabolic reaction, *N*-dealkylation. M7 was determined to be the most abundant metabolite, resulting from a demethylation at the aminoimidazole (Figure 4.1).

The five minor metabolites of ceratamine A were identified as M4, M6, and M8-M10. The majority of these metabolites were formed due to two metabolic reactions, most of which also involved a demethylation at the aminoimidazole. When observing metabolite formation, it became apparent that the formation of the minor metabolites was delayed over the first 30 min.

This observation is consistent with secondary metabolites, with the formation of the three major primary metabolites being the rate limiting step.

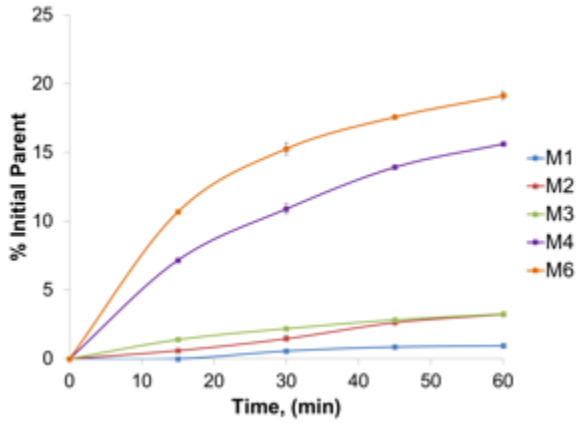

Figure 4.2. Formation of metabolites of ceratamine B in rat liver microsomes.

Figure 4.2 displays the formation of the five phase I metabolites by rat liver microsomes. The most abundant metabolite, M6, was formed as the result of a demethylation at the aminoimidazole, similar to what was observed for ceratamine A. Other similarities were noticed including the fact that the three most abundant metabolites were the result of a single metabolic reaction and that the two secondary metabolites were very minor with delayed formation.

4.2 SEMI-QUANTITATIVE EVALUATION OF THE METABOLISM OF THE CERATAMINES IN HUMAN LIVER MICROSOMES

A total of six phase I metabolites were identified in incubations of ceratamine A with human liver microsomes (0.01 nmol P450/mg protein). Initial analysis was performed using HPLC

coupled with UV detection (Figure 4.3). Similarities in retention times suggested that these six metabolites may be consistent with those already identified in rat liver microsomal incubations. QqTOF MS was utilized to confirm these observations by comparing the precursor and product ions of each metabolite.

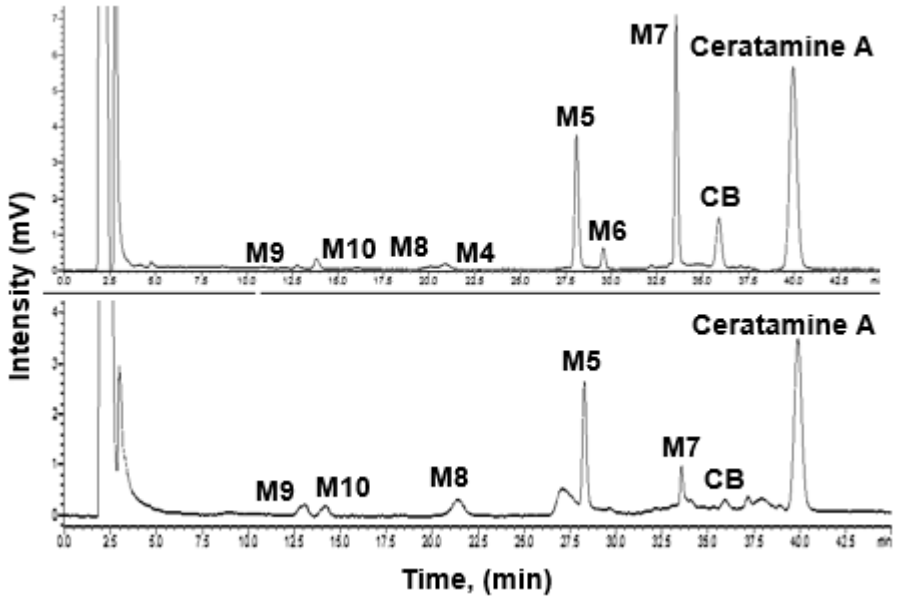

Figure 4.3. RP-HPLC-UV chromatograms of (A) t=60 min incubation of ceratamine A with rat liver microsomes (0.01 nmol P450/mg protein), (B) t=60 min incubation of ceratamine A with human liver microsomes (0.01 nmol P450/mg protein).

The earliest eluting metabolite had molecular ions appearing as a cluster of three ion signals with a 1:3:1 intensity ratio. These precursor ions had *m/z* values of 469, 471, 473, a gain of 2 Da when compared to ceratamine A (Figure 4.4). The major product ion, *m/z* 189, indicated the loss of 14 Da from the imidazoazepinone moiety (Figure 4.4). These characteristics are consistent with those previously observed for M9, which was formed as a result of a demethylation at the aminoimidazole and a monooxygenation along the aromatic ring.

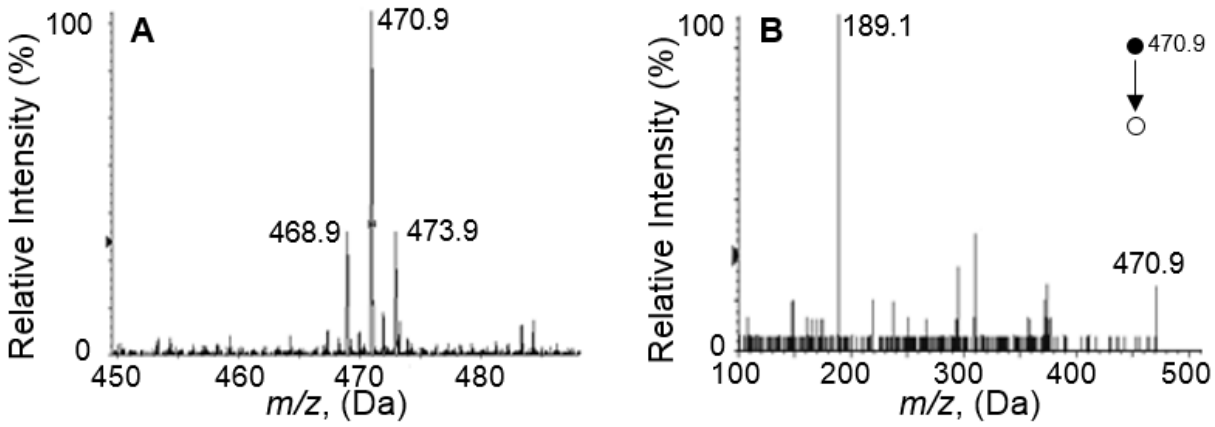

Figure 4.4. (A) $[M+H]^+$ ion clusters and (B) major CID product ion of M9 formed by human liver microsomes.

The second eluting metabolite was found to have precursor ions with *m/z* values of 439, 441, and 443 (Appendix A, Figure A4). This metabolite has an overall mass difference of −28 Da from ceratamine A. This metabolite fragmented to form the major product ion *m/z* 189 (Appendix A, Figure A4). This supports a demethylation occurring on the imidazoazepinone. The MS-MS data corresponds to the previously identified, M10, resulting from a demethylation at the aminoimidazole and methoxy.

The third eluting metabolite of ceratamine A formed by human liver microsomes had a retention time of 21.3 min. The molecular ions had *m/z* values of 483, 485, 487, a gain of 16 Da, suggesting a monooxygenation (Figure 4.5). The major product ion of this metabolite had an *m/z* value of 203, indicating no structural change to the imidazoazepinone (Figure 4.5). These MS-MS characteristics are consistent with M8, which has been previously proposed to result from a monooxygenation along the aromatic ring.

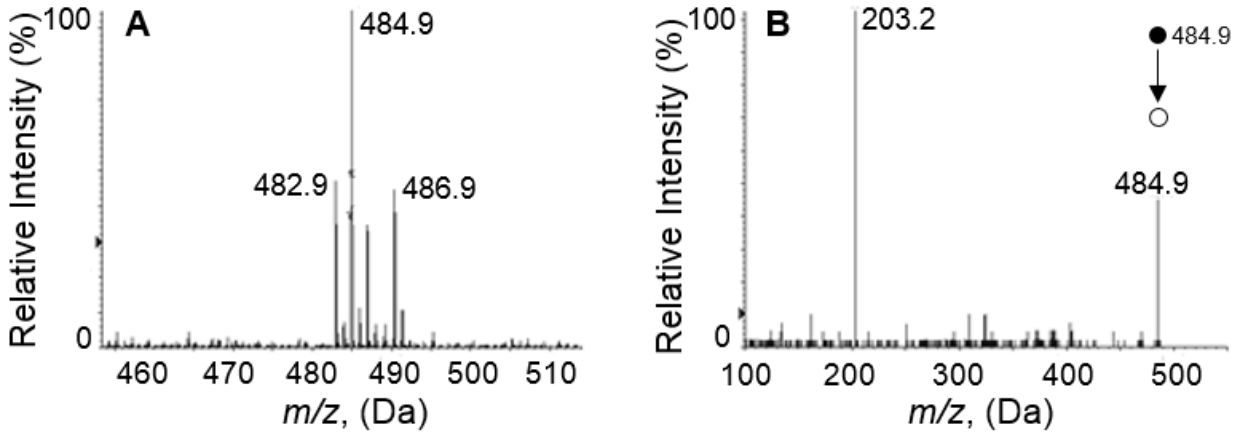

Figure 4.5. (A) $[M+H]^+$ ion clusters and (B) major CID product ion of M8 formed by human liver microsomes.

The final three detected metabolites had retention times of 28.3, 33.5, and 35.9 min. These metabolites were isobaric with precursor ions having *m/z* values of 453, 455, 457, a loss of 14 Da (Figure 4.6). The major product ions were found to be *m/z* 203, 189, and 189, respectively (Figure 4.6). Based on elution order and MS-MS characteristics, these metabolites were found to be consistent with M5, M7, and CB, being formed as a result of a single demethylation at the methoxy (M5), aminoimidazole (M7), or tertiary amide (CB).

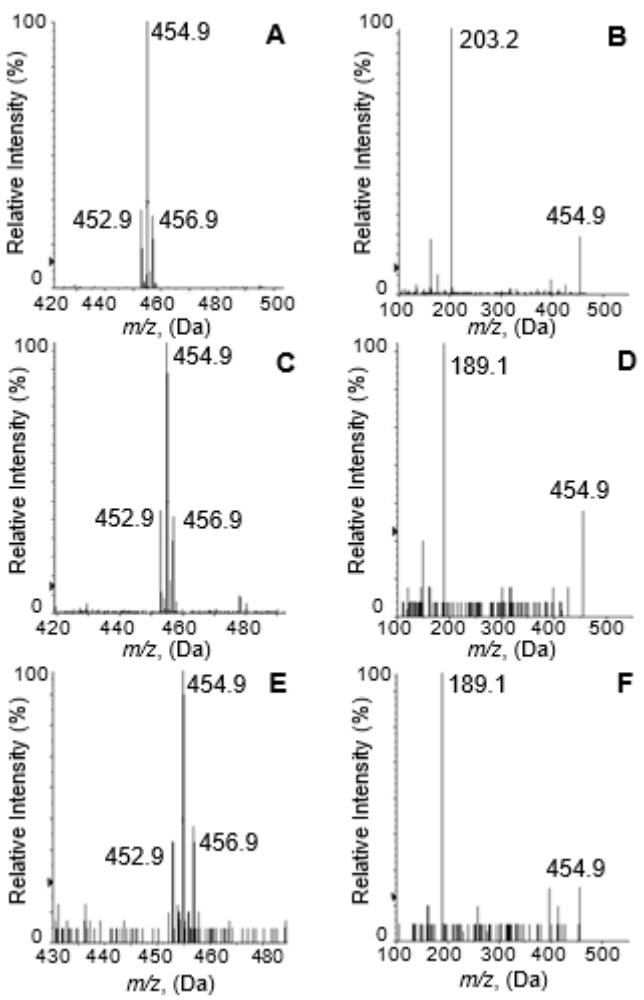

Figure 4.6. (A)$[M+H]^+$ of M5, (B) major CID product ion of M5, (C) $[M+H]^+$ of M7, (D) major CID product ion of M7, (E) $[M+H]^+$ of CB, (F) major CID product ion of CB.

The formation of these six metabolites was monitored over 60 min (Figure 4.7). In terms of abundances, only one major metabolite was observed for ceratamine A in human liver microsomes. This metabolite was identified as M5. The remaining five metabolites were each responsible for approximately less than a 5% loss of the initial control.

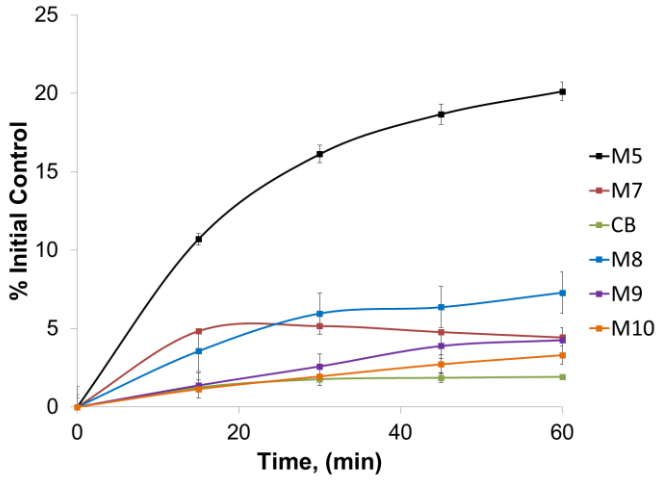

Figure 4.7. Formation of metabolites of ceratamine A in human liver microsomes (0.01 nmol P450/mg protein).

HPLC-UV analysis suggested the formation of four phase I metabolites of ceratamine B by human liver microsomes. The retention times of these metabolites were similar to those formed by rat liver microsomes (Figure 4.8).

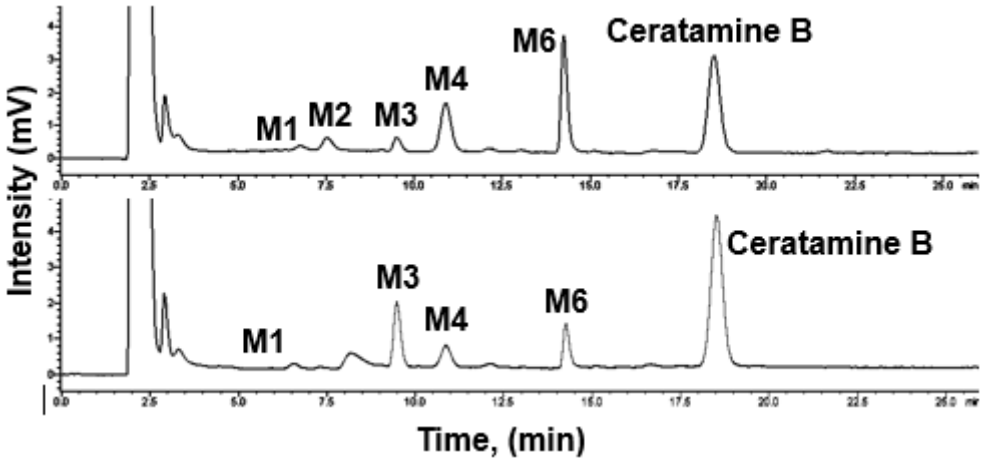

Figure 4.8. RP-HPLC-UV chromatograms of (A) t=60 min incubation of ceratamine B with rat liver microsomes (0.01 nmol P450/mg protein), (B) t=60 min incubation of ceratamine B with human liver microsomes (0.01 nmol P450/mg protein).

Tandem mass spectrometry was used to confirm if these four metabolites are consistent with those previously identified. The metabolite with the shortest retention time had precursor ions with *m/z* values of 453, 455, 457 (Figure 4.9). This mass change of +2 Da had been previously observed and most likely is the result of a demethylation (−14 Da) and a monooxygenation (+16 Da). The major product ion was determined to be *m/z* 175, suggesting that the demethylation occurred on the imidazoazepinone (Figure 4.9). These characteristics are consistent with the previously identified metabolite, M1.

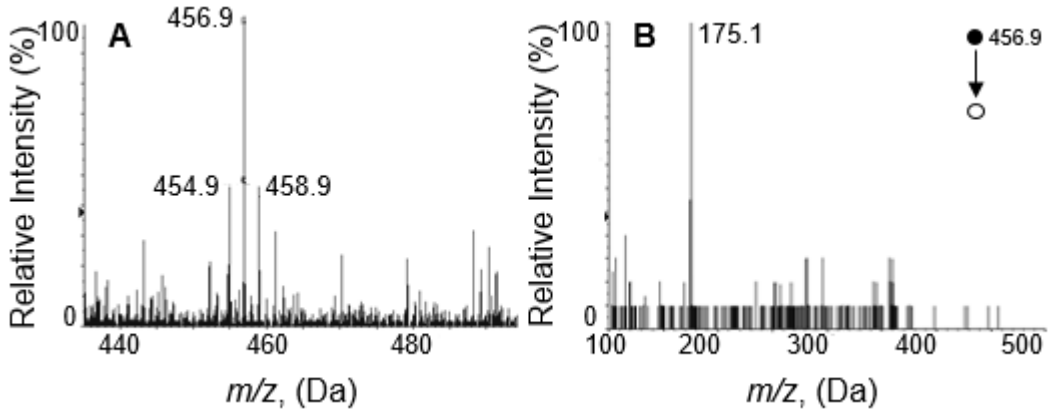

Figure 4.9. (A) $[M+H]^+$ ion clusters and (B) CID product ions of M1 formed by human liver microsomes.

The second metabolite of ceratamine B, formed by human liver microsomes had precursor ions with *m/z* values of 469, 471, 473, a gain of 16 Da (Appendix A, Figure A5). The major product ion was found to have an *m/z* value of 189, supporting that no structural change occurred on the imidazoazepinone (Appendix A, Figure A5). Therefore, this metabolite was identified as M3.

The final two metabolites were found to be isobaric with molecular ions of *m/z* 439, 441, 443, a loss of 14 Da (Figure 4.10). The major product ions were identified as *m/z* 189 and 175, respectively (Figure 4.10). These characteristics were consistent with M4 and M6.

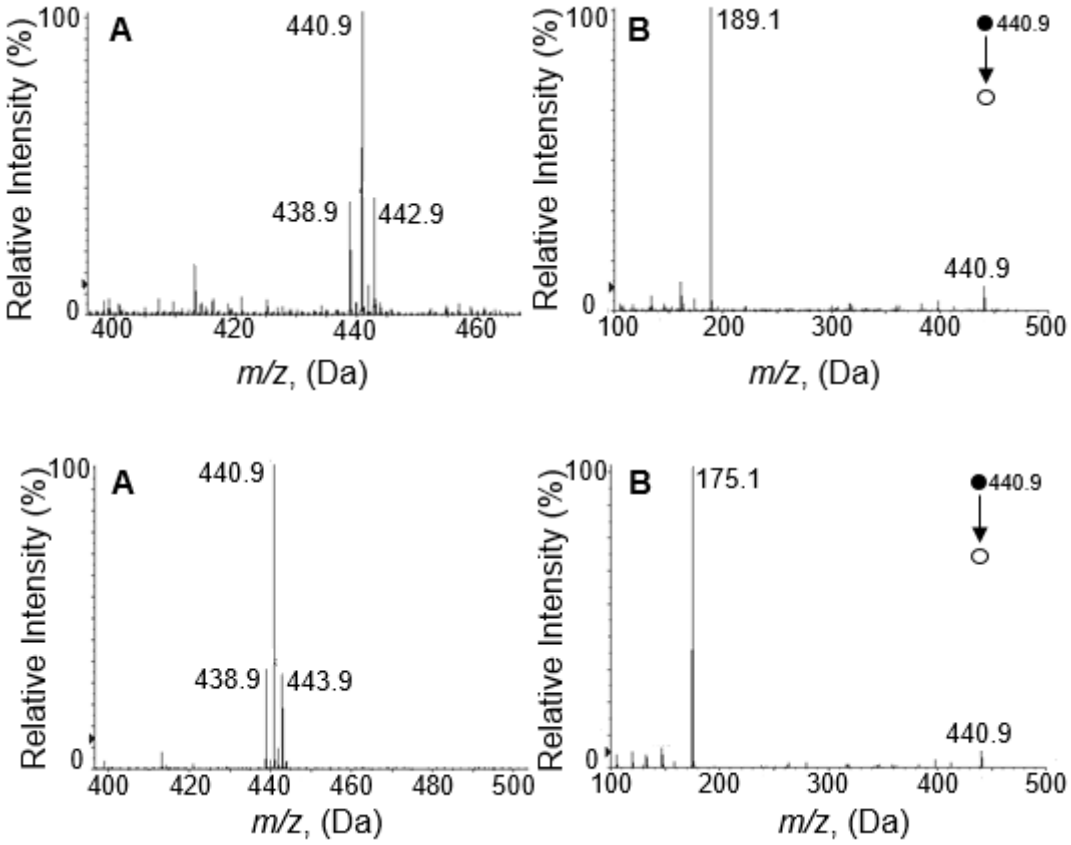

Figure 4.10. (A) $[M+H]^+$ ion clusters of M4, (B) CID product ions of M4, (C) $[M+H]^+$ ion clusters of M6, and (D) CID product ion of M6, formed by human liver microsomes.

The metabolism of ceratamine B in human liver microsomes was also monitored over 60 min (Figure 4.11). The major metabolite was determined to be M3, with 16.3% of the initial control being formed after 60 min of incubation.

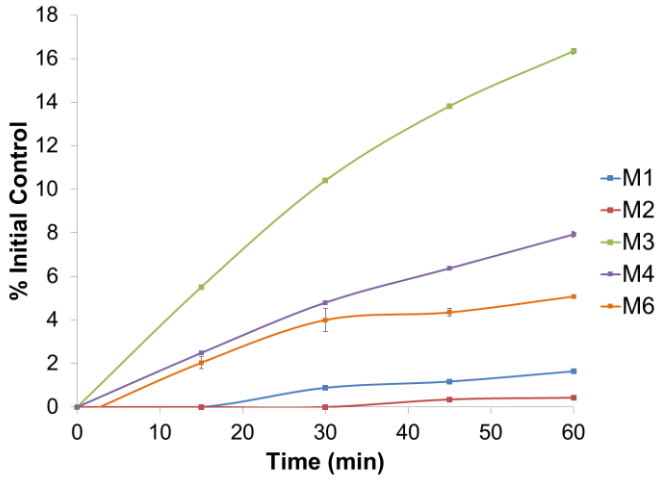

Figure 4.11. Formation of metabolites of ceratamine B in human liver microsomes (0.01 nmol P450/mg protein).

4.3 SPECIES DIFFERENCES IN THE METABOLISM OF THE CERATAMINES

The ceratamines were incubated with human liver microsomes in order to observe any significant species effects on phase I metabolism. All metabolites formed by human liver microsomes were consistent with metabolites already identified in rat liver microsomal incubations. This observation was confirmed by comparison of retention times and LC/MS-MS behavior. Only one major metabolite of ceratamine A was formed by human liver microsomes (Figure 4.12). This metabolite was M5, which was formed as a result of a demethylation at the methoxy. M7 and CB were also detected, however they are both minor metabolites in the human system (Figure 4.12).

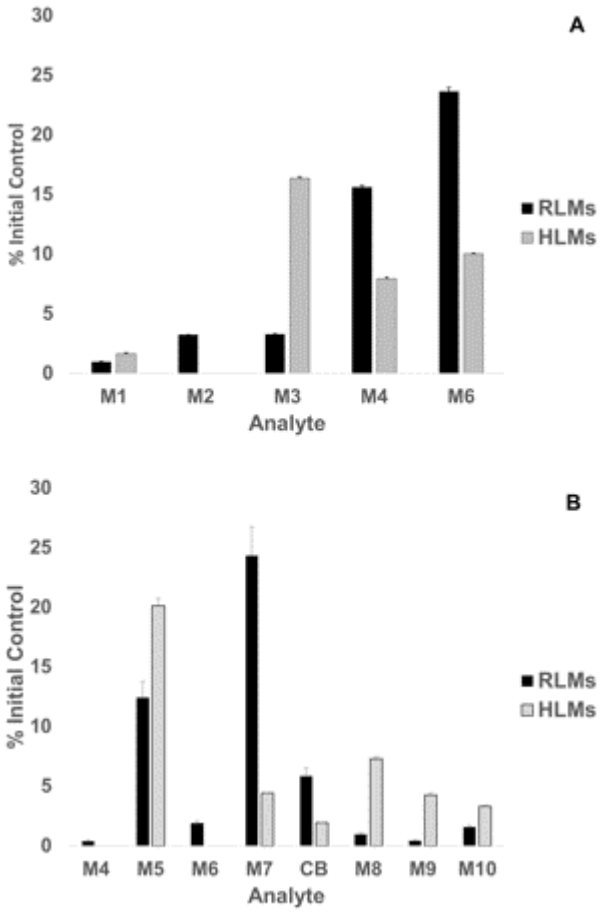

Figure 4.12. Species comparison of the metabolic profiles of (A) ceratamine B and (B) ceratamine A. Incubations were performed with final concentrations of 10 µM drug, 0.01 nmol P450/mg microsomal protein (rat or human liver microsomes), and 1 mM NADPH over 60 min at 37 °C.

A very significant difference in the abundance of metabolites of ceratamine B was noticed in the human liver microsomal incubations (Figure 4.12) The most abundant metabolite was determined to be M3, a very minor metabolite in rat liver microsomes. This metabolite is formed as a result of a monooxygenation, most likely on the dibrominated aromatic moiety, however the specific structure has not been elucidated. M6, the most abundant metabolite in rat liver microsomes, was found to be a minor metabolite in human liver microsomes.

The results of the species comparison suggest that the aminoimidazole is the most metabolically labile site in rat liver microsomes, however the dibrominated aromatic moiety is the preferred site of phase I metabolism in human liver microsomes. The significant species differences in the major metabolites may suggest that a cytochromes P450 subfamily that has been established to have highly variable substrate specificity between species may be involved. Specifically, the CYP2A, CYP2C, and CYP3A families have all been found to have significant species differences in the substrates that they metabolize.[45, 46]

4.4 METABOLIC STABILITY OF THE CERATAMINES

Besides identifying the metabolic profile in multiple species, the evaluation of the metabolic stability of a new drug is also an important part of pre-clinical development. A critical factor in the efficacy of a drug is the amount of that drug that is free (unbound) within the body.[37, 39] This characteristic is commonly referred to as bioavailability and can be significantly influenced by the route of absorption. Oral administration is the preferred method of absorption for new drugs, when possible. The potential of a drug to be orally bioavailable can be evaluated using Lipinski's rules.[39]

According to Lipinski, a drug can likely be considered for oral administration if it has the following characteristics: a molecular weight less than 500 g/mol, a log *P* less than 5, less than 10 hydrogen bond acceptors, and less than 5 hydrogen bond donors.[39]

When examining the structures of the ceratamines it is apparent that they would be predicted to have an oral bioavailability according to Lipinski's rules (Table 4.1). Both compounds are smaller than 500 g/mol, have fewer than 10 hydrogen bond acceptors, and fewer

than 5 hydrogen bond donors. The log *P* has not been experimentally determined for either of the ceratamines but they have predicted values of 2.5 and 1.8 for ceratamine A and B, respectively. The predicted log *P* values were estimated using the XLogP3-AA algorithm via Pubchem.[47-49]

Table 4.1. Lipinski's rule characteristics of the ceratamines.[47, 48]

Analyte	Molecular Weight (g/mol)	Log *P*	Number of Hydrogen Bond Acceptors	Number of Hydrogen Bond Donors
Ceratamine A	468.14	2.5	3	1
Ceratamine B	454.12	1.8	3	2

Since the ceratamines have structural characteristics supporting oral administration, it is essential to investigate their metabolic stability in liver microsomes. Drugs that are taken orally pass directly to the liver via portal circulation, where they undergo initial metabolism before being distributed throughout the body.[37, 39] This process, commonly referred to as first pass metabolism, typically involves phase I metabolic reactions, therefore liver microsomes are an appropriate enzyme system for the evaluation of metabolic stability.[37, 39] If a compound is found to be highly cleared in liver microsomes, it may suggest that oral administration is not warranted.

4.4.1 Metabolic stability of the ceratamines in rat liver microsomes

In order to properly evaluate the metabolic stability of the ceratamines in rat liver microsomes, a simple and robust assay was developed. Optimization and validation was accomplished using four control compounds: propranolol, verapamil, metoprolol, and warfarin. These compounds were chosen based on their range of intrinsic clearance, CL_{int}, values (Table 4.2). To increase the

simplicity of the assay, a single drug concentration of 1 μM was utilized.[48] Using a low drug concentration reduces the risk of performing the assay above the K_M of the majority of drugs, a constant that has not been determined for most lead compounds at this stage of the process.[50]

Table 4.2. Control compounds used for metabolic stability assay in rat liver microsomes.

Control	Literature CL_{int} (μL/min/mg)
Propranolol	1000-5000[51]
Verapamil	87-122[52]
Metoprolol	5-38[51]
Warfarin	2-7[53]

n.d.: not detected

Several rat microsomal protein concentrations were investigated to determine the level necessary to observe metabolism of the control compounds at an expected rate. It was determined that a final protein concentration of 1 mg/mL (0.047 nmol P450/mg protein) was optimal for the metabolic stability assay. The depletion of each control compound in rat liver microsomes was then monitored over 90 min (Figure 4.13). Preparing depletion curves for each compound allowed for the determination of the optimal incubation time for the assay.

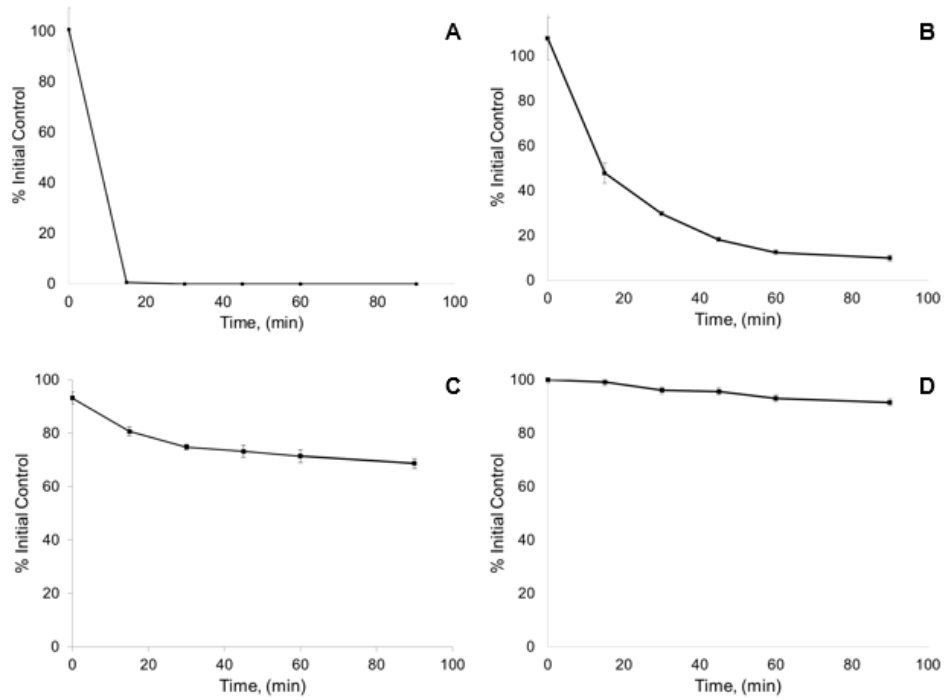

Figure 4.13. Depletion profiles of control compounds used for the validation of the metabolic stability assay in rat liver microsomes: (A) propranolol (high clearance), (B) verapamil (moderate/high clearance), (C) metoprolol (low clearance) and (D) warfarin (low clearance). Incubations were performed with final concentrations of 1 µM drug, 0.047 nmol P450/mg rat liver microsomal protein, and 1 mM NADPH over 90 min at 37 °C.

A 30 min incubation was deemed sufficient to differentiate between drugs with low, moderate, or high clearance categories. The estimation of clearance was determined in a semi-quantitative manner by observing the percentage of the initial control remaining after 30 min. High clearance was defined as <30% remaining, moderate as 30-70% remaining, and low clearance as >70% remaining. The developed assay estimated propranolol as a high clearance control, verapamil as a high-moderate control, and metoprolol and warfarin as low clearance controls; all of which are consistent with literature CL_{int} values.

The reliability of the assay was also evaluated using the control compounds. The intra- and inter-day precision of the assay was typically below 5%, showing acceptable consistency (Table 4.3).

Table 4.3. Validation of metabolic stability assay with rat liver microsomes.

Control	Remaining after 30 min (%)	Intra-day Precision (%)	Inter-day Precision (%)	Clearance Category
Propranolol	n.d.	---	---	High
Verapamil	26.3 ± 2.1	13.9	3.6	High/Moderate
Metoprolol	95.4 ± 2.3	2.3	3.3	Low
Warfarin	89.0 ± 2.9	3.0	5.0	Low

n.d.: not detected

The results of the metabolic stability assay in rat liver microsomes can be seen in table 4.4. After a 30 min incubation, <30% of each of the ceratamines was remaining. Therefore, it was estimated that both ceratamine A and B have high clearance in rats.

4.4.2 Metabolic stability of the ceratamines in human liver microsomes

For the metabolic stability assay in human liver microsomes, nicardipine was utilized as a high clearance control, verapamil was chosen as a moderate clearance control, and propranolol and warfarin were used as low clearance controls (Figure 4.14).

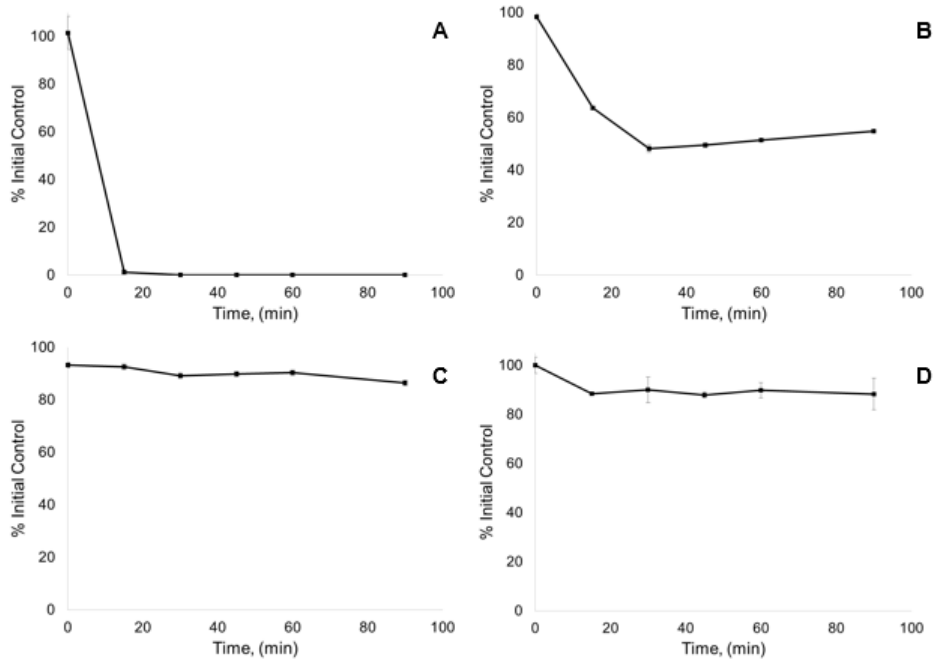

Figure 4.14. Depletion profiles of control compounds used for the validation of the metabolic stability assay in human liver microsomes: (A) nicardipine (high clearance), (B) verapamil (moderate clearance), (C) propranolol (low clearance) and (D) warfarin (low clearance). Incubations were performed with final concentrations of 1 µM drug, 0.047 nmol P450/mg human liver microsomal protein, and 1 mM NADPH over 90 min at 37 °C.

After a 30 min incubation with human liver microsomes, 82.5% was remaining for ceratamine A and 58.8% was remaining for ceratamine B, indicating low and moderate clearance categories for ceratamine A and B, respectively (Table 4.4)

Table 4.4. Clearance categories of the ceratamines estimated by the metabolic stability assay.

	Remaining after 30 min in RLMs (%)	**Clearance Category in RLMs**	**Remaining after 30 min in HLMs (%)**	**Clearance Category in HLMs**
Ceratamine A	10.8 ± 1.3	High	82.5 ± 6.2	Low
Ceratamine B	13.7 ± 0.8	High	58.8 ± 0.5	Moderate

The metabolic stability experiment revealed that both of the ceratamines are rapidly metabolized by rat liver microsomes, however a slower rate of metabolism was observed in human liver microsomes. Although rat systems are commonly used in the study of *in vitro* metabolism of novel drug candidates, significant species differences, particularly between rat and human, have been observed.[54] These differences are typically the result of variations in isoform composition, expression, inhibitory effects, and/or catalytic activities.[54, 55]

The determination of species differences in either metabolic profile or stability is important information to be gathered in early drug discovery.[56] However, the observation of species differences does not necessarily deem a chemical entity a failure as a drug. There are many approved and successful drugs that have been found to have substantial metabolism differences between species during pre-clinical assessments.[57, 58] Compounds such as pregnenolone-16α-carbonitrile (PCN) or the antibiotic rifampicin, are both metabolized at very different rates by rats and humans as a result of variations in the induction of the major metabolizing family, CYP3A. PCN effectively induces CYP3A in rats, however it is unable to increase the expression of human CYP3A, thus it is not significantly metabolized. Conversely, rifampicin has been found to be an inducer of CYP3A in humans but not in rats, explaining the significant difference in metabolic stability between the two species.[57]

Finally, the previously introduced microtubule stabilizer, paclitaxel, is primarily hydroxylated by phase I liver enzymes. The specific site of hydroxylation has been found to differ among several species with the C3'-hydroxy being the predominant metabolite in rats and the 6α-hydroxy in humans.[58]

5.0 IDENTIFICATION OF CYTOCHROMES P450 ISOFORMS INVOLVED IN HUMAN PHASE I METABOLISM OF CERATAMINE B

A final characteristic that is of interest to this pharmacokinetic study is the identification of the specific drug metabolizing enzyme(s) responsible for the formation of the major human phase I metabolites of ceratamine B. The determination of these enzymes can be used to predict the risk of certain drug-drug interactions.[37]

The presence of exogenous compounds, such as xenobiotics, or even many foods, including certain fruits and herbal remedies, can have a significant effect on the activity of drug metabolizing enzymes, either through inhibition or induction.[37] Therefore, the identification of the enzymes involved in the metabolism of a drug can ensure that an individual is not prescribed negatively interacting drugs and is advised on a proper diet to avoid effecting bioavailability due to changes in metabolic clearance.

The focus of this project has been on phase I metabolism, therefore liver microsomes were used as an *in vitro* enzyme system. Although many families of enzymes can be involved in phase I drug metabolism, the majority of phase I metabolic reactions are catalyzed by a superfamily of enzymes known as cytochromes P450.[38] Therefore, the final stage of this study was designed to identify the specific P450 isoform(s) involved. This will be determined using two methods: small molecule inhibition studies and isozyme mapping via recombinant P450s.

5.1 OPTIMIZATION OF CONDITIONS FOR SMALL MOLECULE INHIBITOR STUDIES

Initial studies of ceratamine B metabolite formation were performed with moderate protein concentrations (0.3-0.6 mg/mL). High protein concentrations were avoided in early studies to avoid protein binding, a characteristic that could result in an overestimation of the metabolic stability of ceratamine B. Although metabolism was found to occur at these conditions, the metabolism of ceratamine B was slow with 64.2 ± 0.61% remaining after a 60 min incubation (Figure 5.1).

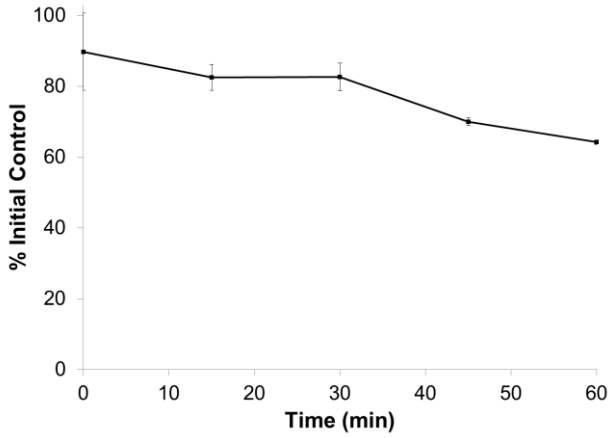

Figure 5.1. Depletion profile of ceratamine B in 0.01 nmol P450/mg protein human liver microsomes.

Another observation made from the initial metabolite formation studies was the lack of linearity, with metabolite formation plateauing between 15 and 30 min (Figure 4.2). In order to use human liver microsomes for the small molecule inhibition studies, conditions needed to be optimized so that the rate of metabolism increases allowing for more metabolite formation, and more importantly, this increased formation occurs in a linear manner. Initial optimization was performed using rat liver microsomes and then transferred over to human liver microsomes.

Increasing total P450 content was found to have a significant effect on the rate of metabolism. Figure 5.2 displays the formation of M2 by rat liver microsomes over 60 min using 3 different total P450 concentrations: 0.01, 0.024, and 0.047 nmol P450/mg protein. Significant differences in the rate of formation were observed within the first 30 min.

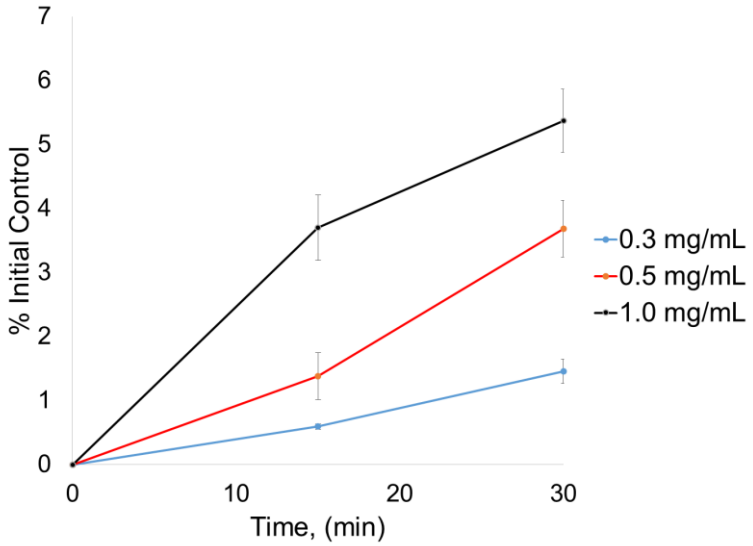

Figure 5.2. Effect of total P450 content on the rate of formation of M2.

Although higher P450 content increased metabolism rate, it did not improve linearity of metabolite formation. The plateau effect that has been observed indicates a lack of substrate or co-factor, either of which would prevent the formation of additional metabolite. Since substrate was always remaining after 60 min incubations with all total P450 concentrations analyzed, it was determined that a lack of co-factor was responsible for non-linearity of metabolite formation. In prior incubations, a single addition of NADPH (1 mM final concentration) was used to initiate the reaction. Increasing the final concentration of NADPH to 2 mM was found to only slightly increase the depletion of ceratamine B in rat liver microsomes (Figure 5.3) This suggested that the cofactor may not be stable over the entire incubation time. An additional incubation was performed using a final concentration of 1 mM NADPH, however two additions

of co-factor were performed (t=0 and t=15 min). The use of multiple additions of NADPH was found to approximately double the depletion of ceratamine B in rat liver microsomes (Figure 5.3).

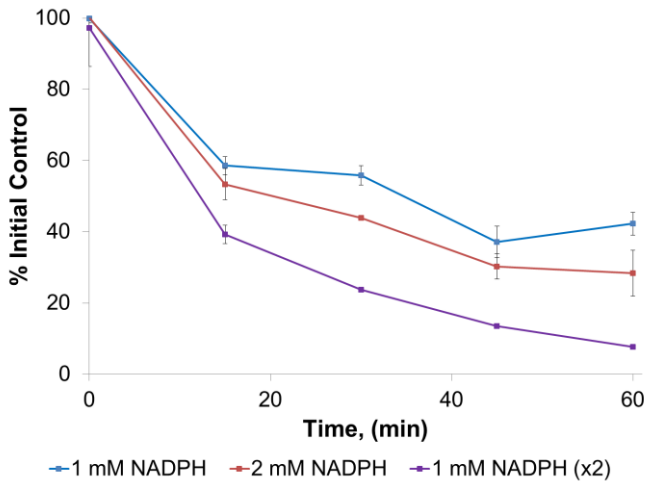

Figure 5.3. Effect of NADPH on depletion of ceratamine B in rat liver microsomes.

Figure 5.4 displays the depletion of ceratamine B and the formation of the three most abundant metabolites, M3, M4, and M6, in human liver microsomes using the optimized conditions. The depletion of ceratamine B was found to be linear over 60 min. The formation of M3 and M4 was linear over 45 min, while the formation of M6 was linear over 30 min. The small molecule inhibitor studies will be performed as a single time point assay (30 min) with a drug concentration of 10 µM, a total P450 content of 0.047 nmol P450/mg protein, and 1 mM NADPH added at t=0 and t=15 min.

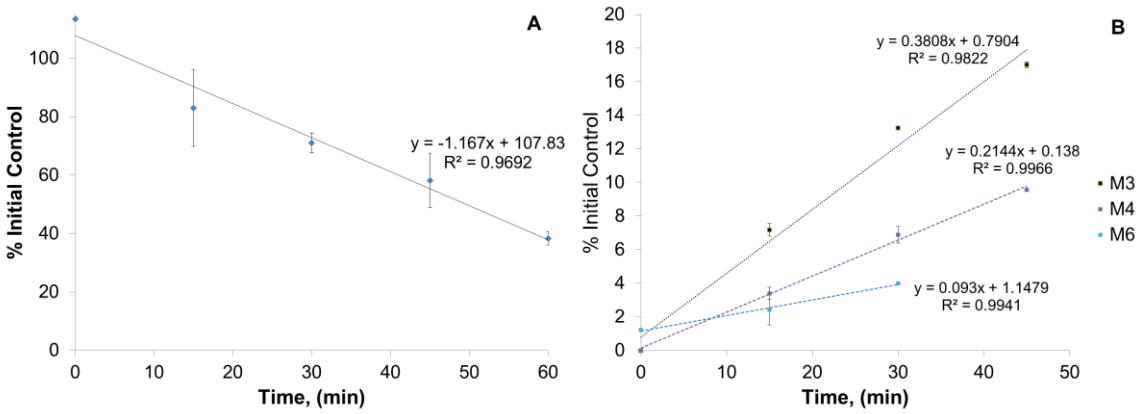

Figure 5.4. (A) Depletion of ceratamine over 60 min of incubation, (B) formation of M3, M4, and M6 over 60 min of incubation. Incubation conditions were performed with final concentrations of 10 µM ceratamine B, 0.047 nmol P450/mg human liver microsomal protein, and 1 mM NADPH (added at t=0 and t=15 min).

5.2 EFFECT OF 1-AMINOBENZOTRIAZOLE ON HUMAN PHASE I METABOLISM OF CERATAMINE B

Cytochromes P450 are a large class of enzymes that are involved in both endogenous and xenobiotic metabolism. Specifically, they are responsible for more than 75% of all drug metabolism.[37] As the focus of this pharmacokinetic study is on phase I metabolism, it is likely that the formation of the major metabolites of ceratamine B in human liver microsomes are catalyzed by P450s. This hypothesis can be tested using the small molecule inhibitor, 1-aminobenzotriazole (ABT).

ABT is a non-specific mechanism-based or suicide inhibitor of cytochromes P450. It is metabolized to a reactive intermediate that irreversibly binds with the porphyrin moiety of the prosthetic heme located in the active site of the enzyme, resulting in the inactivation of the catalytic site.[59]

Following a pre-incubation of ABT with human liver microsomes, incubations were performed using conditions within the linear range in order to observe the effect of ABT on the formation of the three most abundant metabolites of ceratamine B: M3, M4, and M6. The presence of ABT significantly inhibited the formation of M3 and M4, however no effect was observed for M6 (Figure 5.5). These results suggest that M3 and M4 are cytochromes P450 mediated, however M6 is not.

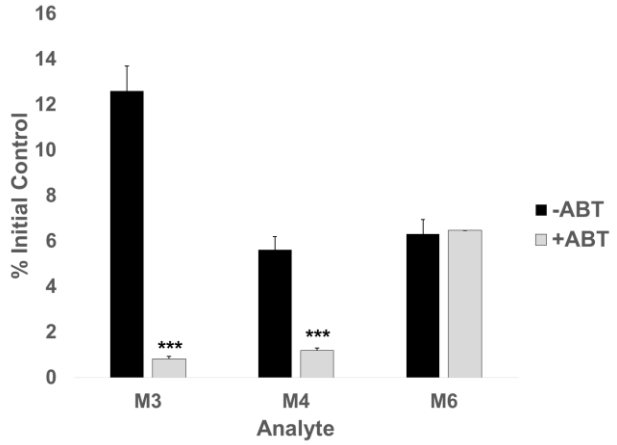

Figure 5.5. Effect of the non-specific cytochromes P450 inhibitor, 1-aminobenzotriazole (ABT), on the formation of the major metabolites of ceratamine B in human liver microsomes. Incubations were performed with final concentrations of 10 µM ceratamine B, 500 µM ABT, 0.047 nmol P450/mg human liver microsomal protein, and 1 mM NADPH for 30 min at 37 °C. ABT was preincubated with microsomes for 20 min prior to reaction initiation.

In order to further investigate the type of enzyme responsible for the formation of M6, additional control incubations were performed (Figure 5.6). M6 was detected within incubations with active human liver microsomes in the absence of NADPH and in incubations of boiled human liver microsomes in the presence of NADPH. When semi-quantitatively compared to the amount of M6 in the active sample, the relative abundance within the controls was considered

minute. This supports that the majority of M6 formation is mediated by an unknown NADPH-requiring enzyme that would be present within the human microsomal fraction. Flavin monooxygenases (FMOs) are the second most commonly involved class of enzymes in the phase I metabolism of xenobiotics.[37] Specifically, there are two FMO isoforms commonly found within the liver, FMO-3 and FMO-5.[37] Although the involvement of FMOs in the formation of M6 has not been directly investigated, due to the abundance of FMOs within the human liver and their requirement of NADPH for activity, their potential involvement in the metabolism of ceratamine B should be investigated in the future.

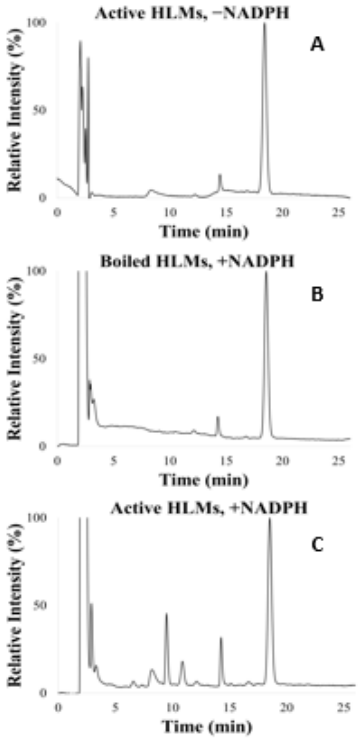

Figure 5.6. RP-HPLC chromatograms of incubations of ceratamine B with (A) active human liver microsomes in the absence of NADPH; (B) boiled human liver microsomes in the presence of NADPH; (C) active human liver microsomes in the presence of NADPH. Incubations were performed with final concentrations of 10 μM ceratamine B, 0.047 nmol P450/mg human liver microsomal protein, and 1 mM NADPH (for boiled control and sample only) for 30 min at 37 °C.

5.3 IDENTIFICATION OF P450 ISOFORMS INVOLVED IN THE FORMATION OF M3 AND M4

Once it had been determined that M3 and M4 are formed by cytochromes P450, an experiment was designed in order to identify the specific isoforms involved in metabolite formation. Initially, isozyme mapping was used as a preliminary screen. Ceratamine B was incubated with nine different isoforms: CYP1A2, CYP2C8, CYP2C9, CYP2C18, CYP2C19, CYP2D6, CYP2E1, CYP3A4, and CYP3A5. These specific isozymes were chosen based on their involvement in xenobiotic metabolism and their abundance in the human liver. Based on the results of the isozyme mapping experiment, incubations with specific small molecule inhibitors were performed in order to confirm the identification of the P450 isoforms involved.

5.3.1 Isozyme mapping

The isozyme mapping experiment revealed that the CYP3A family is responsible for the formation of both M3 and M4 in human liver microsomes (Figure 5.7). For the most abundant metabolite, M3, both isoforms (CYP3A4 and CYP3A5) were significantly involved in the formation, however for M4, CYP3A5 was found to be responsible for the majority of formation. As isoforms within the same subfamily, CYP3A4 and CYP3A5 are very similar, with a structural homology >97%. Although they are thought to be capable of metabolizing similar substrates, their abundances significantly differ within the liver, with CYP3A4 being the major hepato-expressed isoform. The expression of CYP3A5 in the liver is typically very low, however it has been found to be highly variable. Approximately one third of Caucasians have been found to express CYP3A5 within the liver, while this expression is increased within the African-

American population where up to 50% express CYP3A5. Therefore the observation that CYP3A5 is the major enzyme involved in the formation of M4 may suggest significant differences in first pass clearance of ceratamine B across different races.[60]

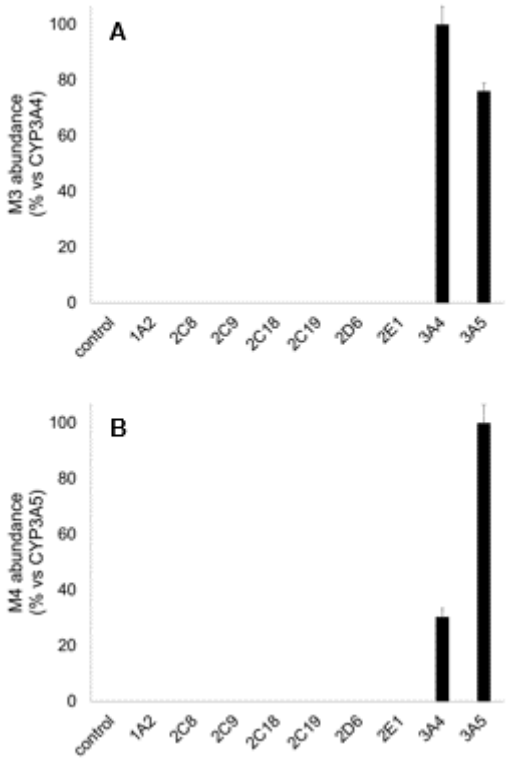

Figure 5.7. Isozyme mapping of the formation of (A) M3 and (B) M4. Incubations were performed with 10 μM ceratamine B, recombinant P450, and 1 mM NADPH for 30 min at 37 °C.

5.3.2 Small molecule inhibition studies

Due to the similarity in the homology of CYP3A4 and CYP3A5, there currently are no known inhibitors specific for each isoform. However, there are several known small molecule inhibitors of the CYP3A subfamily. When used in low concentrations (≤ 1 μM), ketoconazole is an accepted small molecule specific inhibitor of CYP3A.[59] The mechanism of this inhibitor is quite

complex, however it has been determined to be due to both non-competitive and competitive inhibition.[60] The formation of both M3 and M4 was found to be significantly inhibited by the presence of ketoconazole (Figure 5.8). This observation confirmed that the formation of both M3 and M4 and catalyzed by the major drug metabolizing subfamily CYP3A.

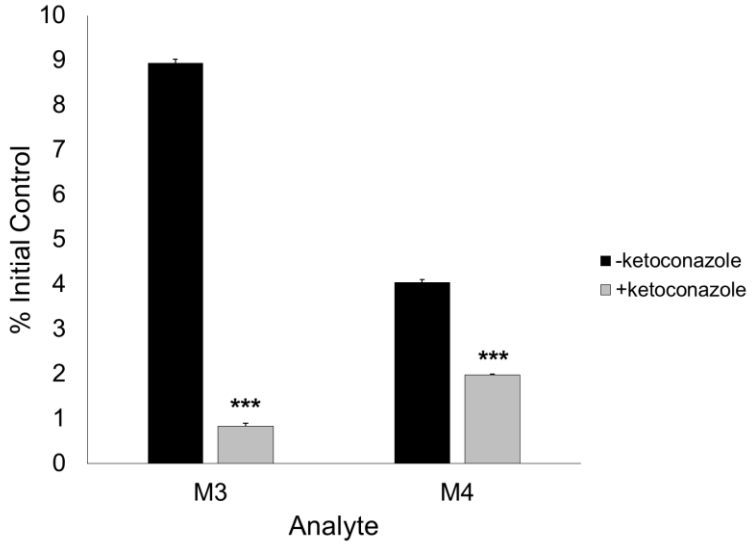

Figure 5.8. Effect of the CYP3A4/5 specific inhibitor, ketoconazole, on the formation of the major metabolites of ceratamine B in human liver microsomes. Incubations were performed with final concentrations of 10 µM ceratamine B, 1 µM ketoconazole, 0.047 nmol P450/mg human liver microsomal protein, and 1 mM NADPH for 30 min at 37 °C.

6.0 CONCLUSION

In conclusion, the ceratamines represent a novel class of structurally simple microtubule perturbagens. They have great potential in the field of cancer drug discovery and possibly in the treatment of various tauopathies, such as Alzheimer's Disease.[29] This work signifies the first pharmacokinetic study of these compounds, greatly contributing to their pre-clinical development. The fate of the ceratamines has been determined in both rat and human liver microsomes. A thorough structure evaluation was performed using a variety of analytical techniques including LC-MS/MS, UV spectroscopy, and NMR spectroscopy. The phase I metabolites were determined to form as the result of *N*-dealkylation, *O*-dealkylation, and/or monooxygenation along the dibrominated aromatic moiety. A species comparison revealed significant differences in the preferred site of metabolism. In rats, the major metabolites for each of the ceratamines resulted from a demethylation at the aminoimidazole, suggesting this is the most metabolically labile site. However, in human liver microsomes the major metabolites for each compound both involved structural changes on the dibrominated aromatic moiety.

An assay was also developed in order to estimate the metabolic stability of the ceratamines in rat and human liver microsomes. Ceratamines A and B were both found to have a high clearance in rats, however they were observed to be more stable in human liver microsomes, with an estimated clearance category of low and moderate, for ceratamine A and B respectively.

Finally, the formation of the two major metabolites of ceratamine B in human liver microsomes were both determined to be cytochromes P450 mediated. An isozyme mapping experiment with various recombinant P450s suggested that the major drug metabolizing subfamily, CYP3A, was responsible for the formation of both metabolites. This was confirmed by performing incubations with the CYP3A specific small molecule inhibitor, ketoconazole.

7.0 FUTURE DIRECTIONS

Based on the initial investigation of the metabolism of each compound, the conclusion of this study is that the ceratamines are potential drug candidates for the treatment of cancer and perhaps tauopathies. Although the results of this project have made significant contributions to the development of the ceratamines as drugs, due to the highly collaborative nature of the drug discovery process, there is a plethora of additional studies that need to be performed.

The interest in the development of the ceratamines can be attributed to their unique, yet simple, structures and the fact that they do not compete for the taxol binding site, suggesting the possibility of use in combination therapies to overcome the challenge of acquired drug resistance. The potential of the ceratamines as a substrate for the P-glycoprotein efflux pump and their ability to penetrate the blood-brain barrier (BBB) should also be evaluated. If they are found to not be substrates of P-glycoprotein and can cross the BBB, their pre-clinical development could gain even more momentum. The identification of the specific binding site of the ceratamines within tubulin is also of great importance as this may reveal a novel binding pocket that can be used as a target for the discovery of additional microtubule stabilizers.

In terms of pre-clinical development there are numerous studies that could be performed. These include the expansion of metabolism studies, comprising those that investigate phase II metabolism and the use of *in vitro* systems that have a higher *in vivo* correlation such as human hepatocytes and precision cut liver slices. The major metabolites identified within each species

analyzed should also be evaluated for biological activity and toxicity. These studies could reveal if the structures of the ceratamines need to be further optimized before reaching clinical development. Finally, the effect of the ceratamines on the activity of major drug metabolizing enzymes should also be investigated, allowing for the prediction of additional drug-drug interactions.

APPENDIX A

Table A1. Accurate mass determinations of major fragments of the ceratamines.

Analyte	Molecular Formula	Theoretical accurate *m/z*	Observed accurate *m/z*	Error (ppm)
Ceratamine A	$C_{10}H_{11}N_4O^+$	203.0927	203.0923	2.2
Ceratamine B	$C_9H_9N_4O^+$	189.0771	189.0785	7.5

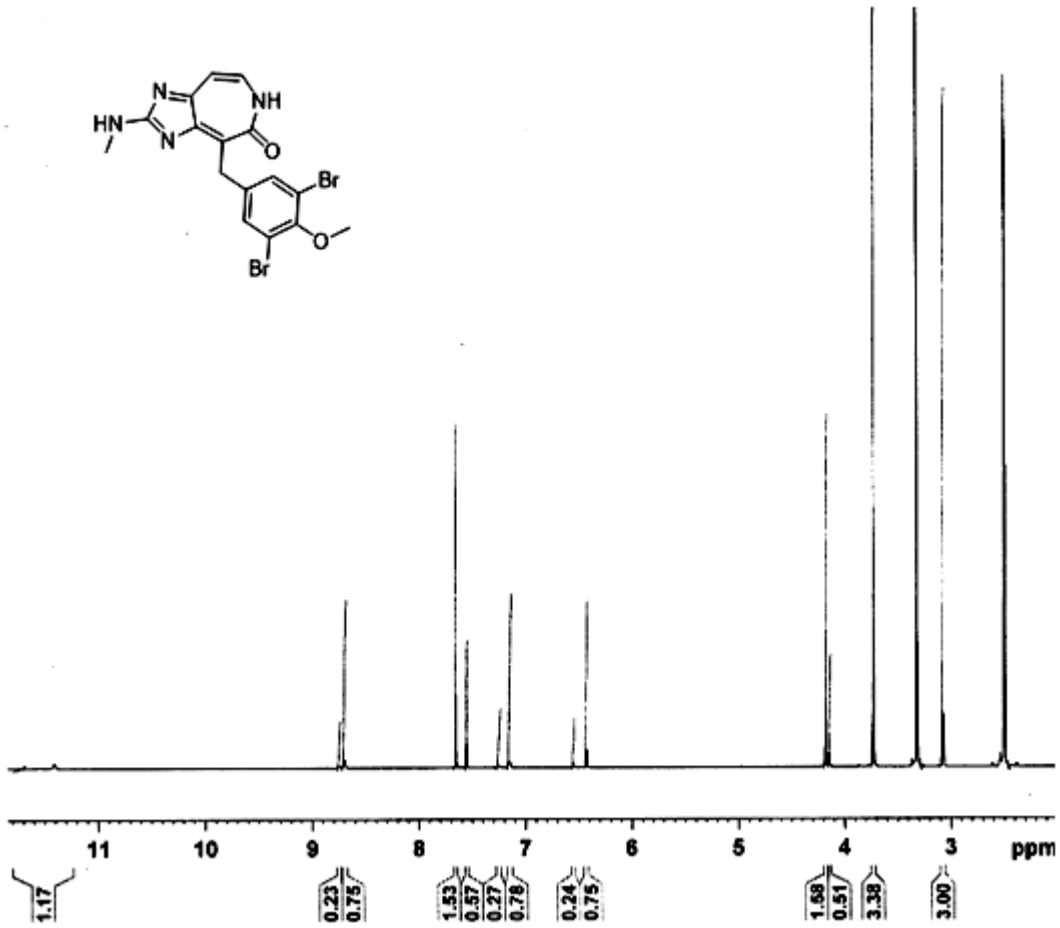

Figure A1. ^{1}H NMR (600 MHz) spectrum of ceratamine B in DMSO-d_6.

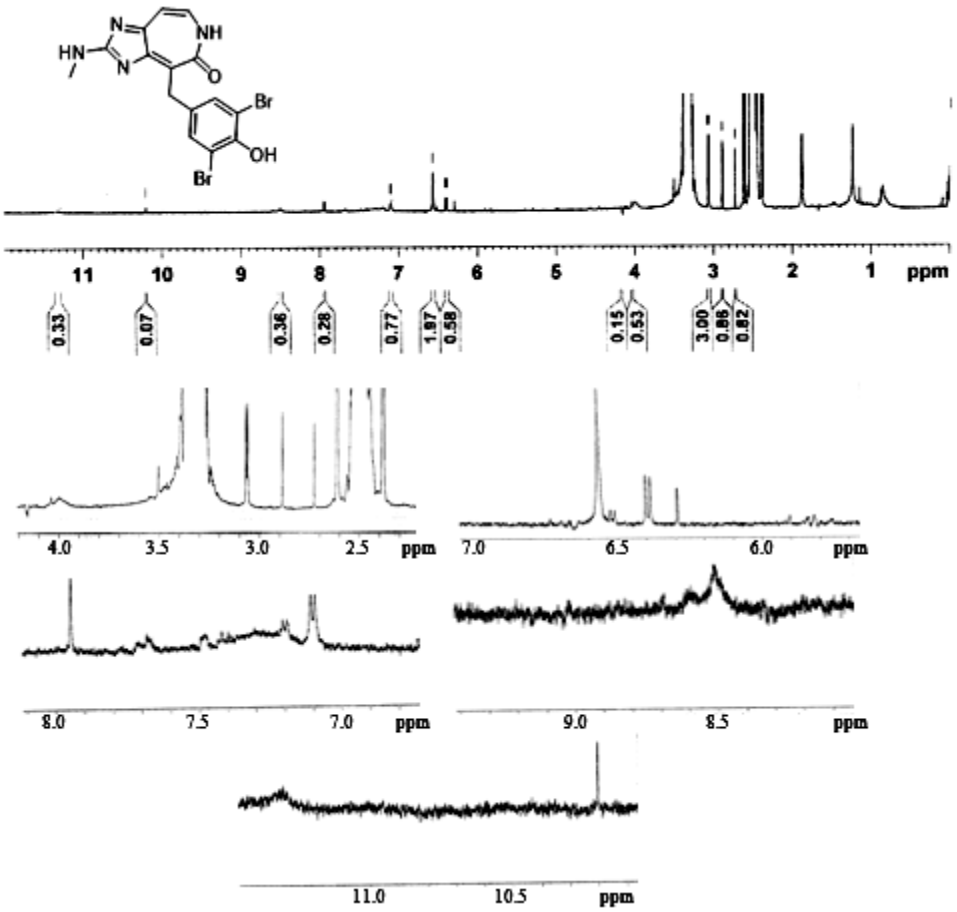

Figure A2. ^{1}H NMR (600 MHz) spectrum of M4 in DMSO-d_6.

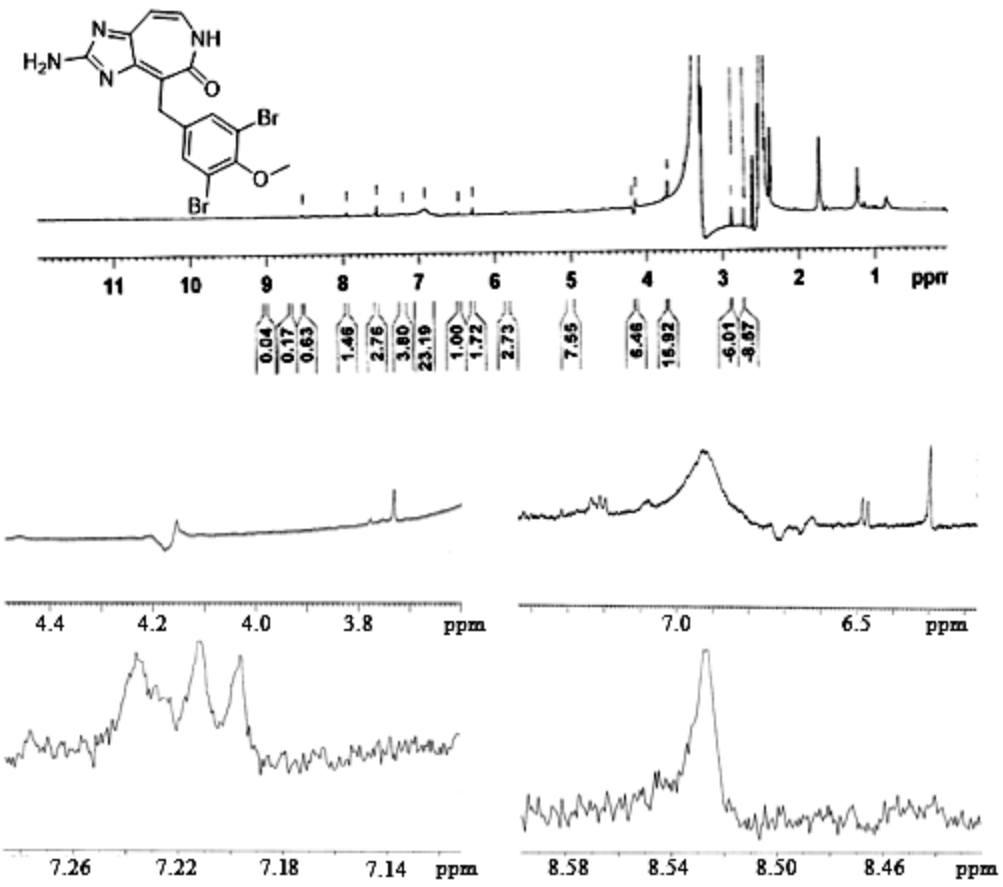

Figure A3. ^{1}H NMR (600 MHz) spectrum of M6 in DMSO-d_6.

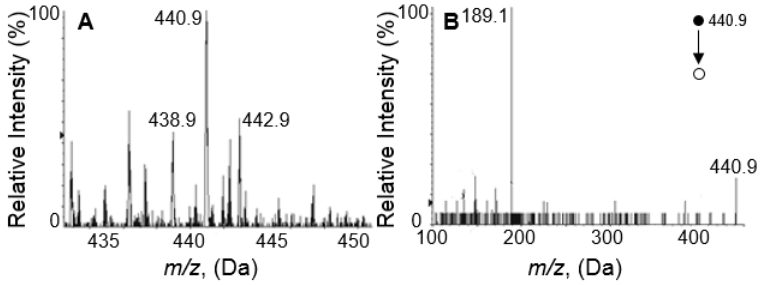

Figure A4. (A) $[M+H]^+$ ion clusters and (B) CID product ions of M10 formed by human liver microsomes.

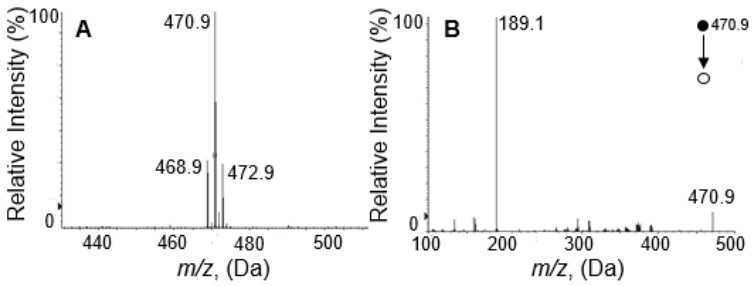

Figure A5. (A) $[M+H]^+$ ion clusters and (B) CID product ions of M3 formed by human liver microsomes.

REFERENCES

1. Li, J. and Vederas, J., *Science*, **2009**, *325*, 161-165.
2. Newman, D.J., *J. Nat. Prod.*, **2004**, *67*, 1216-1238.
3. Molinski, T.; Dalisay, D.; Lievens, S.; Saludes, J., *Nat. Rev.*, **2009**, *8*, 69-85.
4. Carte, B., *BioScience*, **1996**, *46*, 271-286.
5. Usami, Y. *Mar. Drugs*, **2009**, *7*, 314-330.
6. Haefner, B., *Drug Discovery Today*, **2003**, *8*, 536-544.
7. Nastrucci, C.; Cesario, A.; Russo, P., *Recent Patents in Anticancer Drug Discovery*, **2012**, *7*, 218-232.
8. Jordan, M.; Wilson, L., *Nat. Rev. Cancer*, **2004**, *4*, 253-265.
9. Cooper, G., *The Cell: A molecular approach*, 2nd ed., Sunderland, MA, **2000**.
10. Nogales, E.; Wolf, S.; Downing, K., *Nature*, **1998**, *391*, 199-203.
11. Conde, C. and Cáceres, A., *Nat Rev Neurosci*, **2009**, *9*, 319-332.
12. Kirschner, M.; Mitchison, T., *Cell*, **1986**, *45*, 329-342.
13. Amos, L., *Curr. Opin. Struct. Biol.*, **2000**, *10*, 236-241.
14. Ravelli, R.; Gigant, B.; Curmi, P.; Jourdain, I.; Lachkar, S.; Sobel, A.; Knossow, M., *Nature*, **2004**, *428*, 198-202.
15. Roychowdhury, S.; Panda, D.; Wilson, L.; Rasenick, M., *J. Biol. Chem.*, **1999**, *274*, 13485-13490.
16. Wittman, T; Hyman, A.; Desai, A., *Nat. Cell Biol.*, **2001**, 3, 28-34.
17. Walczak, C.; Cai, S.; Khodjakov, A., *Nat Rev Mol Cell Biol*, **2010**, *11*, 91-102.
18. Gigant, B.; Wang, C.; Ravelli, R.; Roussi, F.; Steinmetz, M.; Curmi, P.; Sobel, A.; Knossow, M., *Nature*, **2005**, *435*, 519-522.
19. Löwe, J.; Li, H.; Downing, K.; Nogales, E., *J. Mol. Biol.*, **2001**, *313*, 1045-1057.
20. Bhattacharyya, B.; Panda, D.; Gupta, S.; Banerjee, M., *Med. Res. Rev.*, **2008**, *28*, 155-183.
21. Cragg, G., *Med. Res. Rev.*, **1998**, *18*, 315-331.
22. Han, Y.; Malak, H.; Chaudhary, A.; Chordia, M.; Kingston, D.; Bane, S., *Biochemistry*, **1998**, *37*, 6636-6644.
23. Hari, M.; Loganzo, F.; Annable, T.; Tan, X.; Musto, S.; Morilla, D.; Nettles, J.; Snyder, J.; Greenberger, L., *Mol. Cancer Ther.*, **2006**, *5*, 270-278.
24. Checci, P.; Nettles, J.; Zhou, J.; Snyder, J.; Joshi, H., *TRENDS Pharmacol. Sci.*, **2003**, *24*, 361-365
25. Mitchison, T., *Mol Biol Cell*, **2012**, *23*, 1-6.
26. Orr, G.; Verdier-Pinard, P.; McDaid, H.; Horwitz, S., *Oncogene*, **2003**, *22*, 7280-7295.
27. Yin, S.; Bhattacharya, R.; Cabral, F., *Mol Cancer Ther*, **2010**, *9*, 327-335.
28. Gottesman, M., *Annu Rev Med*, **2002**, *53*, 615-627.

29. Ballatore, C.; Brunden, K.; Huryn, D.; Trojanowski, J.; Lee, V.; Smith, A., *J. Med. Chem.*, **2012**, *55*, 8979-8996.
30. Roberge, M.; Cinel, B.; Anderson, H.; Lim, L.; Jiang, X.; Xu, L.; Bigg, C.; Kelly, M.; Andersen, R., *Cancer Res.*, **2000**, *60*, 5052-5058.
31. Manzo, E.; Van Soest, R.; Matainaho, L.; Roberge, M.; Andersen, R., *Org. Lett.*, **2003**, *5*, 4591-4594.
32. Koehn, F.; Carter, G., *Nat. Rev. Drug Discovery*, **2005**, *4*, 206-220.
33. Karjala, G.; Can, Q.; Manzo, E.; Andersen, R.; Roberge, M., *Cancer Res.*, **2005**, *65*, 3040-3043.
34. Hall, D.; Minton, A., *Anal. Biochem.*, **2005**, *345*, 198-213.
35. Coleman, R.; Campbell, E.; Carper, D., *Org. Lett.*, **2009**, *11*, 2133-2136.
36. Bell, S., *Forensic Chemistry*, Prentice Hall, **2005**.
37. Coleman, M., *Human Drug Metabolism: An Introduction*, Wiley, 1st ed., **2005**.
38. Levine, B., *Principles of Forensic Toxicology*, American Association for Clinical Chemistry, 2nd ed., **2006**.
39. Thomas, G., *Medicinal Chemistry*; John Wiley & Sons Ltd.: West Sussex, England, **2007**.
40. Josephy, P.; Mannervik, B., *Molecular Toxicology*, Oxford University Press, 2nd ed., **2006**.
41. Hariparsad, N.; Sane, R.; Strom, S.; Desai, P., *Toxicol. in Vitro*, **2006**, *20*, 135-153.
42. Brandon, E.; Raap, C.; Meijerman, I.; Beijnen, J.; Schellens, J., *Toxicol. Appl. Pharmacol.*, **2003**, *189*, 233-246.
43. Smith, S.; Dello Buono, M.; Carper D.; Coleman, R.; Day, B.; *J. Nat. Prod.*, **2014**, *77*, 1572-1578.
44. Pasto, D.; Johnson, C., *Organic Structure Determination*; Prentice-Hall, Inc.: Englewood Cliffs, NJ, **1969**, p. 83-108.
45. Martignoni, M.; Groothuis, G.; de Kanter, R., *Exp Opin Drug Met Tox*, **2006**, *26*, 875-894.
46. Guengerich, F., *Chem-Biol Interact*, **1997**, *106*, 161-182.
47. NCBI PubChem Compound: Ceratamine A Chemical and Physical Properties, http://pubchem.ncbi.nlm.nih.gov/summary/summary.cgi?cid=11488186&loc=ec_rcs#x27 website accessed: 06/17/2014.
48. NCBI PubChem Compound: Ceratamine B Chemical and Physical Properties, http://pubchem.ncbi.nlm.nih.gov/summary/summary.cgi?cid=11201846&loc=ec_rcs#x27 website accessed: 06/17/2014.
49. Cheng, T.; Zhao, Y.; Li, X.; Lin, F.; Xu, Y.; Zhang, X.; Li, Y.; Wang, R., *J. Chem. Inf. Model*, **2007**, *47*, 2140-2148.
50. Di, L.; Kerns, E.; Hong, Y.; Kleintop, T.; McConnel, O.; Huryn, D., *J. Biomol. Screen*, **2003**, *8*, 453-462.
51. Komura, H.; Kawase, A.; Masahiro, I., *J. Pharm. Sci.*, **2005**, *94*, 2656-2666.
52. Chen GM, Hu N, Xie SS, Wang P, Li J, Xie L, Wang GJ, Liu XD, *Xenobiotica*, **2011**, *11*, *494*-500.
53. Hermans, J. and Thijssen, H., *Xenobiotica*, **1991**, *21*, 295-307.
54. Jones, S.; Moore, L.; Shenk, J.; Wisely, G.; Hamilton, G.; McKee, D.; Tomkinson, N.; LeCluyse, E.; Lambert, M.; Wilson, T.; Kliewer, S.; Moore, J., *Mol Endocrinol*, **2000**, *14*, 27-39.
55. Xie W., Structure and function of PXR and CAR in *Nuclear Receptors in Drug Metabolism*, John Wiley & Sons, Inc., Hoboken, NJ., **2006**, p 147-164.
56. Zhang, D.; Luo, G.; Ding, X.; Lu, C., *Acta Pharmaceutica Sinica B*, **2012**, *2*, 549-561.

57. Nassar, A., *Drug Metabolism Handbook: Concepts and Applications*, John Wiley & Sons. Hoboken, NJ, **2009**, p. 461.
58. Vaclavikova, R.; Soucek, P.; Svobodova, L.; Ansenbacher, P.; Simek, P.; Guengerich, F.; Gut, I., *Drug Metab and Dispos*, **2004**, *32*, 666-674.
59. Ortiz de Montellano, P. and Mathews, J., *Biochem. J.*, **1981**, *195*, 761-764.
60. Williams, J.; Ring, B.; Cantrell, V.; Jones, D.; Eckstein, J.; Ruterbories, K.; Hamman, M.; Hall, S.; Wrighton, S., *Drug Metab. Dispos.*, **2002**, *30*, 883-891.
61. Khojasteh, S.; Prabhu, S.; Kenny, J.; Halladay, J.; Lu, A., *Eur. J. Drug Metab. Pharmacokinet.*, **2011**, *36*, 1-16.
62. Greenblatt, D.; Zhao, Y.; Venkatakrishnan, K.; Duan, S.; Harmatz, J.; Parent, S.; Court, M.; von Moltke, L., *J. Pharm. Pharmacol.*, **2011**, *63*, 214-221.